Theor Chim Acta (1991) 78: 287–326

Theoretica Chimica Acta

The ring opening of cyclopropylidene to allene: global features of the reaction surface

P. Valtazanos, S. T. Elbert, S. Xantheas*, and K. Ruedenberg

Ames Laboratory, USDOE**, and Department of Chemistry, Iowa State University, Ames, IA 50011, USA

Received March 1, 1986; received in revised form August 30, 1990/Accepted September 15, 1990

Summary. The global features of the groundstate ring opening of cyclopropylidene to allene are studied by means of *ab-initio* FORS MCSCF calculations based on a minimal AO basis set. The energy surface is completely mapped out in terms of three reaction coordinates, namely the CCC ring-opening angle and two angles describing the rotations of the CH_2 groups. For each choice of these three variables, the twelve remaining internal coordinates are optimized by energy minimization. In the initial phase of the reaction, as the CCC angle opens, the CH_2 groups rotate in a disrotatory manner, maintaining C_s symmetry. This uphill reaction path leads to a transition region which occurs early, for a CCC angle of about 84°. In this transition region the reaction path branches into two pathways which are each others' mirror images. The system exhibits thus a *bifurcating transition region.* Passed this region, the two pathways are overall conrotatory in character. However, these downhill reaction paths to the products are poorly defined because, from a CCC opening angle of about 90° on, *the CH_2 groups can rotate freely and isoenergetically in a synchronized, cogwheel-like manner* and this disrotatory motion can mix unpredictably with the conrotatory downhill motion. There is no preference for any one of the two reaction pathways yielding the two stereoisomers of allene and the reaction is therefore *nonstereospecific* with respect to the numbered hydrogen atoms. The global surface is documented by means of contour maps representing slices corresponding to constant CCC angles. The bifurcating transition region is mapped in detail.

Key words: Cyclopropylidene to allene – Bifurcating transition region – Strained rings – Potential energy surface – Contour maps

* *Present address:* Molecular Sciences Research Center, Pacific Northwest Laboratory, Richland, WA 99352, USA

** Operated for the U.S. Department of Energy by Iowa State University under Contract No. 7405-ENG-82. This work was supported by the office of Basic Energy Sciences

1. Introduction

The isomerization of cyclopropylidene to allene:

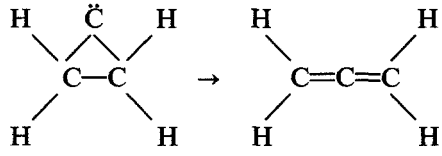

is a reaction of interest in organic chemistry because the reactant is the simplest carbene undergoing CC bond fission due to ring strain. Strained rings play a considerable role in the understanding of basic organic chemical concepts. Carbenes, on the other hand, with their low-lying singlets and triplets and their electrophilic as well as nucleophilic properties are one of the less-well-understood reaction intermediates. A reliable understanding of the pathway of this prototype reaction has therefore fundamental implications regarding many complex concerted reactions.

Among the questions regarding which experimentalists expect illumination from theorists are the following. Is cyclopropylidene a (meta)stable species? What is the energy of reaction, what is the activation energy of the ring opening? And in particular, how do the CH_2 groups rotate during the opening of the ring? All such questions are, in principle, answered by the *potential energy surface* governing this ring-opening reaction. The challenge lies not only in its accurate determination but also in extracting the essential information from an energy function depending upon fifteen geometric parameters. As it turns out, this potential energy surface is sufficiently rich in nontrivial features so that it is of interest to map out a considerable part of it. The identification of its significant regions and the accurate determination of its key features form the content of the present series of investigations.

1.1. Experimental findings

Allene is a well-known and stable compound, whose geometry, energy, and other important data are well documented. Lord and Venkatesvarlu [40], Almenningen et al. [1], Maki and Toth [44], and Hegelund et al. [22] all have reported experimental results for allene and a thorough review of these and other experimental and theoretical results is given by Runge [57].

Cyclopropylidene, on the other hand, is a transient metastable species, which has not yet been isolated experimentally in its unsubstituted form. The existing experimental evidence on the stereospecificity implies that the reaction of the *substituted* molecule is at least partially stereospecific. Thus Jones et al. [36], Jones and Wilson [35], Walbrick et al. [71], and Jones and Walbrick [34] all report obtaining more-or-less optically active allene when starting with optically active cyclopropylidene. All their experiments are performed using heavily substituted species and the authors state that the observed partial stereospecificity is most likely due to the bulk of the substituents rather than to any inherent electronic reasons. An exception to this is a more recent communication by Jones and Krause [33], wherein certain experimental results are interpreted as providing evidence for covalent electronic effects playing a role in the formation of one

or the other of the possible stereoisomers. Specifically they point out that if *cis*-2-phenyl-3-*p*-methylphenylcyclopropylidene gives an allene which is partially optically active, then *cis*-2-*p*-bromophenyl-3-*p*-methylphenylcyclopropylidene should give a product which has either *lower* optical purity or a *reversed* configuration, due to the fact that bromine is larger than hydrogen. In actual fact, however, an allene of *higher* optical activity and the *same* relative configuration is obtained, and this result is taken as an indication that effects other than those deriving from steric hindrance, i.e., electronic effects, contribute in determining the product.

There is no experimental evidence regarding the nature of the transition state. As to the activation energy barrier itself, Chapman [7] points out that at temperatures as low as 77 K cyclopropylidene gives allene spontaneously, which would tend to indicate a quite low barrier. Even though the experiment in question is inconclusive and there seems to be some doubt as to whether the true ground state of cyclopropylidene was indeed involved, the fact remains that the reaction always proceeds with ease and consequently the barrier cannot be high.

1.2. Previous theoretical calculations

In view of the slim experimental evidence, there have been a number of attempts to explain theoretically what happens in the course of this reaction. Borden [5] suggested that, for orbital symmetry reasons, the reaction should proceed via a monorotatory path, which means that only one CH_2 group rotates as the CCC angle opens. Bodor et al. [4] using the MINDO/2 semiempirical model, concluded that the ring opens in a nonrotatory fashion (i.e., without rotation of the CH_2 groups) to yield planar D_{2h} allene, which then undergoes internal rotation to give the final D_{2h} product. They calculated the barrier height to be 13.7 kcal/mol and determined that the reaction is exothermic by less than 40 kcal/mol. The transition state (which would have C_{2v} symmetry like cyclopropylidene) was placed at a CCC opening angle of approximately 85°. Dillon and Underwood [9], in a Simplex-INDO semiempirical calculation, found that the reaction starts out as disrotatory, reverses its motion to give a nonrotated transition state, and thereafter continues to its conclusion via a conrotatory path. They placed the transition state at a CCC opening angle of 96°, estimated the barrier to be 72 kcal/mol and the overall exothermicity of the reaction about 25 kcal/mol. Pasto et al. [46], using *ab-initio* methods for the first time, concluded that the conversion involves three distinct processes: first an initial disrotatory opening proceeding almost to the transition state, then a rapid transformation from the disrotatory to distorted monorotatory structure at an opening angle of between 90° and 100°, and finally a nonrotatory conversion of the 100° structure to allene. The transition state was estimated to lie between 90° and 94.5°, the activation energy was calculated to be about 18 kcal/mol, and the overall reaction exothermicity about 74 kcal/mol. It should, however, be noted that in all of the aforementioned investigations extremely severe geometrical restrictions were imposed on the reaction path. As a consequence, Dillon and Underwood [9] did not even find any stable ring structure!

More recently, Honjou et al. [28, 29], using sophisticated *ab-initio* methods, arrived at a barrier of 11 kcal/mol and an overall reaction exothermicity

62.6 kcal/mol. However, they did not attempt to elucidate the reaction pathway nor did they identify the transition state. Rauk et al. [48] made quite extensive calculations using the 3-21G [3] basis at the SCF level to determine geometries and using 6-31G and 6-31G** [21, 23] bases together with third-order Møller–Plesset perturbation theory [45, 47] to improve the energetics. They determined stationary points on the energy surface by analytical gradient techniques and reported a barrier of 11.47 kcal/mol as well as a reaction exothermicity of 64.5 kcal/mol. They estimated the transition state to be asymmetric with a CCC opening angle of 96°.

Some controversy existed regarding the spin multiplicity of the cyclopropylidene ground state. While Dillon and Underwood [9] found singlet cyclopropylidene to be lower than the triplet, Pasto et al. [46] claimed that the triplet is the true ground state. More recent calculations by Stierman and Johnson [67] and Honjou et al. [29, 31] plus minimal and extended basis set geometry optimizations performed in the present work, have however confirmed beyond any reasonable doubt that the singlet is indeed considerably lower in energy.

1.3. Present investigation

As a result of the work reported here, we not only find the intrinsic reaction path but also present a complete map of the energy for the ring opening in terms of three "reaction coordinates", namely the CCC ring-opening angle Φ and two angles δ_1, δ_2 which describe the rotations of the two CH_2 groups. For each $(\Phi, \delta_1, \delta_2)$ triple, all other internal coordinates are completely optimized. In this manner a comprehensive visualization of the reaction path is achieved. Aside from determining the critical points, several special features of this reaction are discovered. First, the reaction has a "bifurcating transition region", i.e., the branching of the reaction path towards the two isomeric products occurs in the vicinity of the transition state. Secondly, after the CCC angle has opened to about 100°, the two CH_2 groups can rotate freely in a synchronized cogwheel-like fashion and, for this reason, there really exists no unique reaction path from the transition state to the products. Finally, the reaction is found to be *not* stereospecific for the unsubstituted compound assuming the hydrogen atoms are distinguished by numbering.

In the present paper we establish the *global* features of the potential energy surface governing this reaction. Because of the magnitude of this task these calculations were performed within the FORS MCSCF framework and using a minimal STO-3G basis of atomic orbitals. In the subsequent paper [74] we develop a conceptual orbital interpretation of the electronic rearrangements which relates the present *ab-initio* results to intuitive chemical thinking. In a third paper [73] we proceed to examine the critical regions of the reaction surface using more accurate calculations with an extended atomic orbital basis and by enlarging the FORS configuration space through the addition of single and double excitations. In the fourth paper [70] the ring-opening reactions of some substituted molecules are considered and it is shown that the stereospecificities found for the substituted cyclopropylidenes can be attributed to steric and long-range electrostatic interactions between the substituents rather than to covalent electronic effects.

2. Theoretical approach

2.1. The FORS model

In view of the computational savings, the use of the SCF approximation could be instructive if the present reaction were dominated by a single configuration throughout. Since such is not the case, a wavefunction with the capacity to adapt to changing dominant configurations is required. This kind of flexibility is provided by the model of the full optimized reaction space (FORS) which combines the inclusion of non-dynamic correlation with the preservation of chemical interpretability. The model was introduced in 1976 by Ruedenberg and Sundberg [56], used by Cheung et al. [8], and further developed by Ruedenberg et al. [54]. It has been applied to a number of reactions by Dombek [10], Feller [18], Johnson and Schmidt [32], Feller et al. [19], Schmidt [60], Lam and Johnson [39], and Lam [38]. The model combines consistently the concept of a full valence space with the principle of orbital optimization and explores systematically the implications of such a framework. The concept has been generalized beyond the valence space by Roos et al. [49, 50, 63, 64] to the "complete active space self-consistent field (CASSCF)" procedure, which has been very successful.

The FORS model describes the electronic structure of a molecule in terms of the best wavefunction that can be obtained by a superposition of all configurations that are generated by *all possible* occupancies and couplings from a "formal minimal basis" of those valence orbitals on the constituent atoms which are actively involved in the reaction. These configurations span the "full reaction space", and MCSCF optimization (see for example Ruedenberg et al. [53] or Yaffe and Goddard [75]) of the orbitals in terms of an extended set of quantitative basis orbitals determines the "full optimized reaction space": FORS.

For the system at hand, Fig. 1 represents a schematic picture of the orbitals of the reactant and the product considered here. There are nine *core orbitals*, which we label $|c_1\rangle \ldots |c_9\rangle$, namely three carbon 1*s* inner shells (not shown), two carbon-carbon sigma bond orbitals and four carbon-hydrogen bond orbitals, all of which are indicated by bond-lines. These core orbitals can be assumed to remain doubly occupied throughout the reaction. Then there are four *reaction orbitals* labeled $|0\rangle$, $|0'\rangle$, $|1\rangle$ and $|2\rangle$ and they are explicitly shown in Fig. 1. They change both in character and occupation as the reaction progresses from the reactant to the products. Thus, for orbital $|0\rangle$ one has a change from σ^2 to π_x^1; for orbital $|0'\rangle$ from π^0 to π_y^1; for orbital $|1\rangle$ from σ^1 to π_x^1; and for orbital $|2\rangle$ from σ^1 to π_y^1 (the superscripts denote occupations). The *actual shapes* of the aforementioned orbitals, as deduced *a posteriori* from the FORS MCSCF calculations, will be exhibited and discussed in detail in the second paper [74]. The FORS wavefunction with 18 core electrons in the 9 core orbitals and 4 reactive electrons in the 4 reaction orbitals embodies all possible rearrangements among the four reactive orbitals and therefore possesses the flexibility needed to account for the configurational changes that can be expected during the progress of the reaction. Since it involves only 20 configurations, it is sufficiently compact to permit the required extensive calculations. Its explicit form is

$$\Psi^{SM} = \Sigma_{Kt} C_{Kt} \Phi_{Kt}^{SM}$$

where each of the 20 configurations Φ_{Kt}^{SM} is a normalized spin-adapted antisymmetrized product (SAAP) of configuration generating orbitals (CGOs), i.e., all MOs that are occupied in any of the configurations of the wavefunction. A

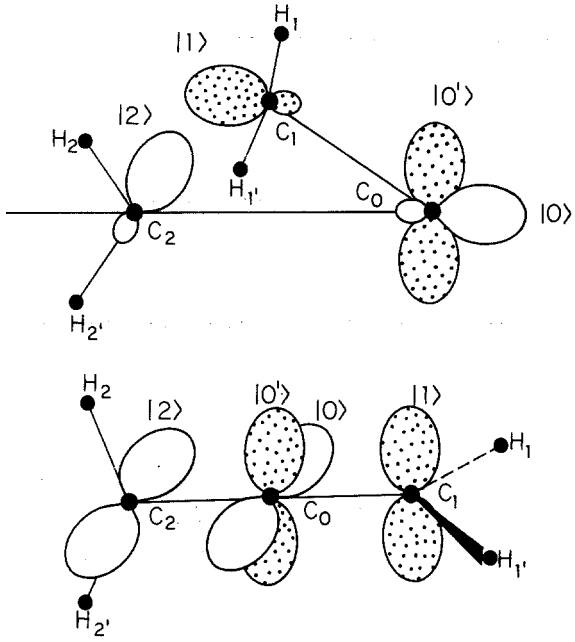

Fig. 1. Qualitative depiction of the reaction orbitals $|0\rangle$, $|0'\rangle$, $|1\rangle$, $|2\rangle$ in cyclopropylidene and allene

SAAP is a normalized N electron wavefunction of the form

$$\Phi_{Kt}^{SM}(\text{space, spin}) = N_K A\{U_K(\text{space})\Theta_t^{SM}(\text{spin})\}$$

where Θ_t^{SM} is a spin eigenfunction, S and M being the eigenvalues of S^2 and S_z; U_K is a product of CGOs; $A = (N!)^{-1/2}\Sigma_p(-1)^p P$ is the conventional antisymmetrizer, and $N_K = 2^{-\pi(K)/2}$ with $\pi(K)$ being the number of doubly occupied CGOs in U_K. Properties of SAAPs are described by Ruedenberg [52], Salmon et al. [58], and Ruedenberg and Poshusta [55].

The ground states of both cyclopropylidene and allene are singlets. Assuming only C_1 symmetry throughout, the full singlet configuration space generated by the four reaction orbitals is spanned by the following 20 SAAPs

$$|i^2j^2\rangle = 2^{-1}A\{\text{Core}\,|i\rangle^2\,|j\rangle^2\Theta_0\}: \quad 6\ \text{SAAPs}$$
$$|i^2jk\rangle = 2^{-1/2}A\{\text{Core}\,|i\rangle^2\,|j\rangle\,|k\rangle\Theta_0\}: \quad 12\ \text{SAAPs}$$
$$|00'12S\rangle = A\{\text{Core}\,|0\rangle\,|0'\rangle\,|1\rangle\,|2\rangle\Theta_0\}: \quad 1\ \text{SAPP}$$
$$|00'12T\rangle = A\{\text{Core}|0\rangle\,|0'\rangle\,|1\rangle\,|2\rangle\Theta_1\}: \quad 1\ \text{SAAP}$$

where

A = antisymmetrizer

i, j, k = all possible choices of 0, 0′, 1, 2

$\Theta_0 = (\alpha\beta - \beta\alpha)(\alpha\beta - \beta\alpha)/2$, singlet coupling spin function

$\Theta_1 = \{\alpha\alpha\beta\beta + \beta\beta\alpha\alpha - (\alpha\beta + \beta\alpha)(\alpha\beta + \beta\alpha)/2\}/\sqrt{3}$, triplet coupling

$\text{Core} = c_1^2c_2^2 \ldots c_9^2(\alpha\beta - \beta\alpha)^9/2^{9/2}$.

2.2. *Atomic orbital basis sets*

As regards the basis of atomic orbitals to be used for the present study, questions of feasibility are decisive since the global surface to be determined requires around ten thousand energy calculations, all of the multi-configuration FORS-MCSCF type. It was therefore decided to obtain the preliminary overview by using the STO-3G minimal basis set of Hehre et al. [24–26, 66] because it is economical and has also been effective in giving reliable geometries, especially for hydrocarbons. The shortcomings of this basis set were subsequently remedied by means of the extended basis set calculations to be reported in the third paper [73].

2.3. *Choice and reduction of internal coordinates*

Since C_3H_4 has 7 atoms, its geometry is fully characterized by 21 Cartesian coordinates. Elimination of the 6 coordinates corresponding to translation and free rotation of the molecule leaves 15 internal coordinates. The full reaction surface is thus a 15 dimensional surface in a 16 dimensional space, namely the energy as a function of 15 independent variables. This poses problems because of the magnitude of the task of calculating such a surface and also because of the difficulty of interpreting it. However, a reduction of the dimensionality of the surface has to be done in such a way that the salient features of the reaction are preserved.

Figure 2 illustrates and defines the 15 internal coordinates that we chose to describe the geometry of the molecule. They are: 6 bond lengths (2 C–C bond lengths and 4 C–H bond lengths), 5 valence angle bends (the 4 C–C–H angles and the C–C–C ring-opening angle Φ), 2 out-of-plane bends (the angle between each C–C bond and the corresponding CH_2 plane), and 2 dihedral angles (the

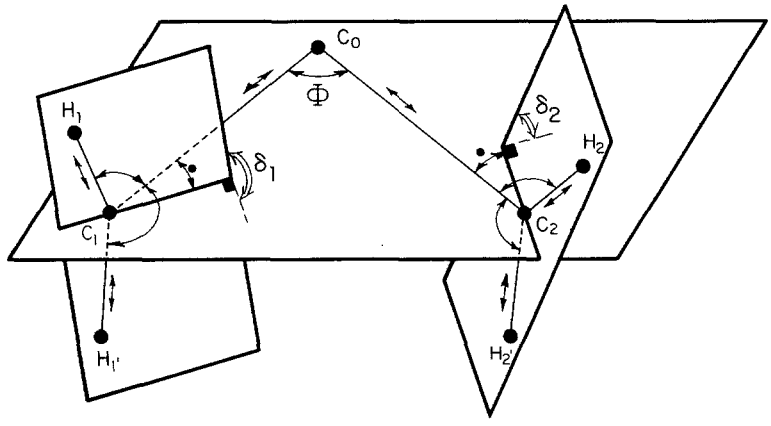

Fig. 2. The 15 internal coordinates of C_3H_4 chosen in this work. (For graphic reasons the dotted curved arrows representing the out-of-plane bends are drawn slightly incorrectly. Rather than pointing to the line of intersection of the CCC plane with the CCH plane, the right end should point to the projection of the CC bond on the CHH plane.) $3 \times 7 - 6 = 15$ internal coordinates in H_2CCCH_2. ↔, Bond stretch (6); , valence angle bend (5); , out of plane bend (2); , dihedral angle of rotation of CH_2 plane vs. C_3 plane (2)

angles between the CCC plane and each of the two CH_2 planes) which we shall call δ_1 and δ_2. It should be noted that, for each of these angles, the two defining planes have only one atom in common so that their line of intersection does not coincide with any bond. Therefore, the two dihedral angles defined in Fig. 2 are not standard torsion angles such as defined for example by Wilson et al. [72]. Of these 15 coordinates, the angles Φ, δ_1, and δ_2 are the most interesting ones for the reaction, because Φ represents the extent of the ring opening, whereas δ_1 and δ_2 can be considered as describing the rotations of the hydrogen pairs around the respective lines of intersection of the CH_2 planes with the CCC plane. We would expect the other twelve internal coordinates to change less drastically during the course of the reaction and this will be verified in Sect. 7. We therefore choose $(\Phi, \delta_1, \delta_2)$ as the "reaction coordinates", i.e., we will follow the reaction explicitly in terms of these three variables. The other twelve internal coordinates will not be ignored, however. For each $(\Phi, \delta_1, \delta_2)$ triple, the geometry will be completely optimized with respect to the remaining twelve variables. We note in particular that the lines of intersection of the CH_2 planes with the CCC plane (i.e., the instant axes of rotation of the CH_2 groups) change along the reaction path as Φ opens up. The choice of reaction coordinates will be reevaluated in Sect. 7.

The geometry optimization with respect to twelve internal coordinates means that, for every set of values for the opening angle Φ and the hydrogen plane twisting dihedral angles δ_1 and δ_2, the molecular energy is minimized with regard to all other nuclear parameters. Thereby these 12 internal coordinates become functions of Φ, δ_1, δ_2 and thus *the energy surface itself becomes a function of these three internal reaction coordinates.* Its form can be visualized in terms of contour surfaces $E(\Phi, \delta_1, \delta_2) = \text{constant}$ which are two-dimensional surfaces in the three-dimensional parameter space spanned by Φ, δ_1, δ_2. For a graphical representation, we found it expedient to display the intersections of these surfaces $E = \text{constant}$ with various planes $\Phi = \text{constant}$. The resulting contour lines $E(\delta_1, \delta_2, \Phi_0) = \text{constant}$, for a fixed value $\Phi = \Phi_0 = \text{constant}$, exhibit the dependence of the energy upon the dihedral rotation angles δ_1, δ_2 for a given value of Φ_0 of the CCC opening angle. The entire energy surface is thus covered by a sequence of such panels corresponding to various values of Φ. The nature of the reaction surface turns out to be such that an adequate description of its pertinent features is obtained by examining about 20 panels corresponding to the following values of the ring-opening angle:

$$\Phi = 50(10)70(5)80(2)82(1)88(2)90(5)100(20)180$$

where the numbers in parentheses indicate step sizes (e.g., 90(5)100 means: 90, 95, 100).

Since δ_1 and δ_2 both can vary from $-180°$ to 180°, it still seems at first sight as if an enormous number of (δ_1, δ_2) points are needed for each panel. However, since the energy is optimized with respect to the remaining 12 coordinates, it is readily seen that, for a given value of Φ, the energy is unchanged (i) when the CH_2 planes are rotated by 180°; (ii) when the molecule is reflected by the CCC plane; (iii) when the left and right parts of the molecule are interchanged. This means that the contours in a plane $\Phi = \text{constant}$ are invariant under the following operations: (i) translation by 180° in the δ_1 direction; (ii) translation by 180° in the δ_2 direction; (iii) inversion, i.e., replacing (δ_1, δ_2) by $(-\delta_1, -\delta_2)$; (iv) exchanging the values of δ_1 and δ_2, i.e., reflection by the line $\delta_1 = \delta_2$. By combining these invariances it follows that the energy has the same value for all

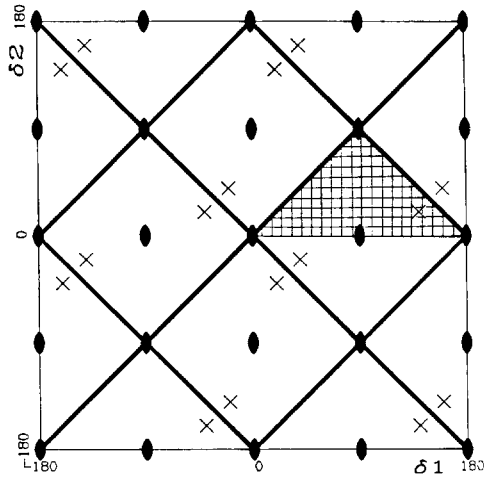

Fig. 3. The two-dimensional space symmetry of the energy surface on a panel Φ = constant. *Crosses* indicate equivalent points. *Ovals* denote diagonal axes. *Heavy diagonal lines* denote reflection planes. *Cross hatched area* indicates primitive region

points indicated by cross marks on the sample panel displayed in Fig. 3 and this implies that the contour map of each panel Φ = constant possesses the two-dimensional lattice symmetry indicated in the same figure. Consequently, it is only necessary to calculate energies for points in a region equivalent to the crosshatched area in the figure, which is 1/16 of the entire panel.

We chose to calculate 55 points in this primitive area in order to obtain good isoenergetic contours. They were taken to be the points given by the values:

$$\delta_1 = 20n_1 + 10n_2, \qquad \delta_2 = 10n_2$$
$$n_1 = 0, 1, 2 \ldots (9 - n_2), \qquad n_2 = 0, 1, 2, \ldots, 9.$$

As mentioned before, each of the 55 points involves a minimization with respect to the other 12 internal coordinates.

From these 55 energy values on any one panel, those for the 880 equivalent points on the entire area shown in Fig. 3 were generated by symmetry and they were used to draw energy contours using a standard interpolation procedure. An analytical expression of the energy could be obtained by determining the appropriate Fourier expansion for each panel and, then, expressing the Fourier coefficients in terms of suitable functions of Φ.

Finally, it is useful to realize how the point representing the system progresses on a Φ = constant panel when the two CH_2 groups rotate in a "disrotatory" or "conrotatory" manner while the three carbon atoms remain fixed. It is readily seen that such synchronized motions are represented by following straight lines with slopes at $\pm 45°$ on a panel Φ = constant. Four particular cases which will be important in the sequel are illustrated in Fig. 4. For the further analysis it is also expedient to consider, in place of δ_1, δ_2, a set of alternative coordinates which describe motions parallel to the lines shown in Fig. 4, namely:

(a) the average conrotatory angle $\delta_+ = (\delta_1 + \delta_2)/2 - 90°$ and

(b) the average disrotatory angle $\delta_- = (\delta_1 - \delta_2)/2$.

These internal coordinates are further discussed and illustrated below in Section 3.

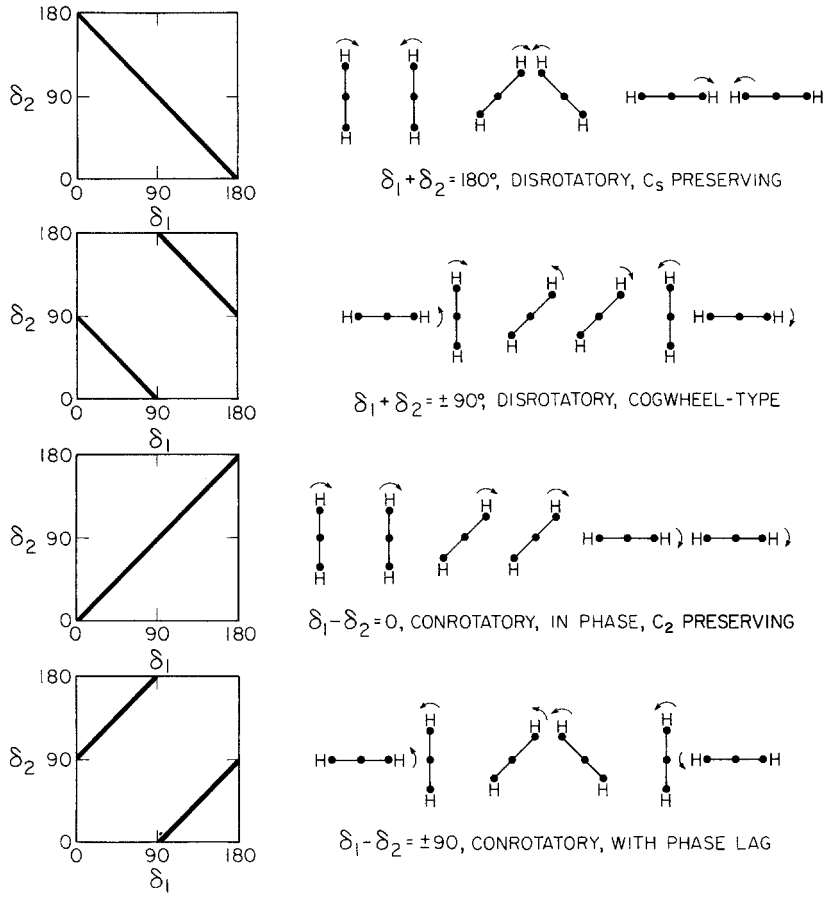

Fig. 4. Representation of disrotatory and conrotatory motions on a panel Φ = constant

2.4. Implementation

An efficient means of optimizing geometries is the gradient method developed by McIver and Komornicki [42, 43] and implemented as a computer algorithm by Dupuis and King [11]. It uses the energy gradient with respect to the geometric coordinates as a guide to the steepest descent path towards the energy minimum (optimum geometry). Dupuis et al. [12] incorporated this method into the GAMESS (general atomic and molecular electronic structure system) MCSCF computer program. This program was heavily modified by M.W. Schmidt of North Dakota State University and S.T. Elbert of the Ames Laboratory, USDOE, Iowa State University. It incorporates, for example, Schlegel's [59] geometry optimization and saddle point location algorithm. We furthermore developed and implemented the necessary algorithm for the aforementioned new internal coordinate, namely the dihedral angle between two planes having only one point in common [17]. This was done in analogy to the standard treatment as given, for example, by Wilson et al. [72].

As mentioned above, the energies for 55 points (δ_1, δ_2) on each of the 19 panels (Φ = const.) had to be determined, i.e., a total of about one thousand energy values. For each of these thousand points the energy had to be minimized with respect to the other twelve internal coordinates. Since the gradient procedure requires on the average about a dozen evaluations of the molecular energy with a given set of the 15 internal coordinates, the determination of the entire energy surface involves approximately 19 panels × 55 points/panel × 12 energies/point = 13,000 evaluations of the molecular energy. Each of these energy calculations is a multiconfiguration-self-consistent-field calculation involving 20 configurations based on 9 inactive and 4 active molecular orbitals.

The calculations were performed on a VAX 11/780 computer.

3. The intrinsic reaction path

It is customary first to determine the transition state (TS) of a reaction by an appropriate iterative procedure, and then to determine the intrinsic reaction (IRC) path as the union of the steepest descent lines from the transition state to the reactant and product minima. In the present case, the usual methods for finding the transition state fail, because they are based on second-order Taylor expansions. In the STO-3G approximation, there exist two transition states very close to a "valley-ridge inflection" (VRI) point, i.e., in a "bifurcation region" where a fourth-order Taylor expansion is required to obtain a workable approximation [69]. We shall describe the *determination* of these transition states below in Section 6.1.

From these transition states the two intrinsic reaction paths [20] were determined by the steepest descent procedure of Ishido et al. [30], as incorporated into the GAMESS program [12] by Schmidt et al. [61]. The two paths are related to each other by symmetry. Thirteen points of one of them are given in Table 1. Listed are all internal coordinates and the energies. They form the first row of every pair of rows in the table. Graphical representations of the variation of Φ, δ_1, δ_2 for the two reaction paths are shown in Fig. 5. Figure 5a traces the variation of the rotation angles δ_1 and δ_2 along the IRC on a (δ_1, δ_2) panel such as was introduced in Fig. 3. The alternative coordinates δ_+ and δ_- defined at the end of Sect. 2.3 are also shown. At various points along the path the corresponding values of the ring-opening angle Φ are indicated. The following facts are apparent: (i) The reaction path has a bifurcation. While it is known that bifurcations of least-energy steepest descent lines rigorously occur "almost always" at the reactant minima [69], the bifurcation occurs here, *practically speaking*, around 80°; (ii) the bifurcation occurs before the transition state so that there are two transition states; (iii) the transition states and the bifurcation occur quite close to each other. The variations of δ_+ and δ_- as functions of Φ along one of the reaction paths are illustrated by the plots shown in Fig. 5b. For the other path the δ_+ values have the opposite sign. The bifurcation occurs where δ_+ starts to deviate from zero.

For each of the IRC points listed in Table 1, we also performed the following additional calculation: The "primary" coordinates $(\Phi, \delta_1, \delta_2)$ were held fixed and the other twelve "secondary" coordinates were optimized. These calculations gave the results listed in the second row of every pair of rows in Table 1. (Due to an inadequacy in the program, the values of Φ, δ_1, δ_2 did not always stay *exactly* fixed during these optimizations. However, the values listed for the

Table 1. Internal coordinates (see Fig. 2) and energies of points along the IRC path and of geometries which are optimized for points with the same, or very closely the same values of Φ, δ_1, δ_2

	Φ	δ_1	δ_2	r_{01}	r_{02}	r_{11}	$r_{11'}$	$r_{22'}$	α_{011}	$\alpha_{011'}$	α_{022}	$\alpha_{022'}$	β_1	β_2	Energy	Max.grad	
C	59.45	90.0	90.0	1.532	1.532	1.081	1.081	1.081	1.081	117.1	117.1	117.1	117.1	33.1	−33.1	−114.39557	0.0002
	64.75	103.5	76.6	1.506	1.507	1.088	1.085	1.088	1.085	116.6	120.6	116.5	120.8	28.5	−28.4	−114.37890	
	64.75	103.5	76.7	1.499	1.499	1.081	1.080	1.081	1.080	116.7	120.4	116.7	120.5	27.8	−27.6	−114.37947	0.0003
	70.38	112.5	67.8	1.484	1.485	1.083	1.077	1.083	1.077	116.7	124.6	116.5	124.9	20.3	−19.9	−114.36008	
	70.36	111.8	68.4	1.475	1.475	1.082	1.079	1.082	1.079	117.7	112.8	117.5	123.1	20.9	−20.8	−114.36053	0.0002
	74.85	118.6	62.1	1.469	1.470	1.082	1.076	1.082	1.076	117.1	126.5	116.7	127.0	13.8	−13.0	−114.34741	
	74.85	117.9	62.9	1.461	1.461	1.084	1.080	1.084	1.079	118.2	124.5	117.9	125.0	15.1	−14.7	−114.34793	0.0001
	80.25	125.6	56.8	1.452	1.457	1.083	1.078	1.084	1.080	117.9	127.2	117.2	128.1	7.3	−5.3	−114.33724	
	80.25	125.3	57.2	1.449	1.450	1.086	1.081	1.086	1.081	118.4	126.2	117.8	127.2	7.7	−6.4	−114.33773	0.0002
	83.32	132.1	56.0	1.447	1.452	1.083	1.079	1.084	1.083	118.6	126.8	117.7	128.1	5.7	−2.7	−114.33319	
	83.32	131.1	55.4	1.444	1.449	1.087	1.083	1.087	1.083	118.9	126.2	117.7	128.0	5.0	−1.4	−144.33379	0.0002

T	84.24	134.8	57.1	1.448	1.448	1.086	1.081	1.086	1.081	118.3	125.9	117.2	127.1	5.9	−4.0	−114.33199	0.007
	87.73	139.6	57.8	1.428	1.453	1.084	1.081	1.086	1.083	119.3	126.3	118.8	126.5	4.9	1.9	−114.33363	
	87.54	132.3	52.8	1.420	1.507	1.090	1.084	1.090	1.089	119.1	126.1	113.1	125.0	8.7	29.0	−114.33485	0.003
	100.09	157.1	61.5	1.406	1.393	1.078	1.087	1.078	1.084	122.2	121.5	125.4	119.8	3.4	7.3	−114.38745	
	100.09	156.9	61.3	1.435	1.399	1.091	1.087	1.088	1.080	122.5	118.5	122.5	122.1	23.3	13.5	−114.41104	0.0003
	120.02	185.7	68.6	1.375	1.345	1.082	1.086	1.079	1.083	123.1	120.4	127.3	117.0	6.7	4.0	−114.45532	
	120.00	190.3	65.4	1.394	1.356	1.088	1.086	1.083	1.081	120.4	121.4	123.4	120.9	18.6	3.0	−114.45921	0.0002
	140.20	195.6	71.4	1.348	1.334	1.085	1.085	1.086	1.086	122.5	120.3	125.0	118.2	10.4	3.5	−114.48469	
	140.20	195.6	71.3	1.355	1.335	1.084	1.085	1.082	1.082	121.7	120.5	122.9	120.6	14.1	3.9	−114.48537	0.0004
	160.25	200.4	68.9	1.321	1.331	1.074	1.074	1.083	1.090	122.1	121.4	122.6	120.5	6.0	2.4	−114.49523	
	160.25	200.4	68.9	1.328	1.323	1.083	1.083	1.082	1.083	121.8	121.3	122.3	121.0	7.0	2.6	−114.49662	0.00009
A	179.00	202.5	67.5	1.320	1.320	1.083	1.083	1.083	1.084	121.5	121.5	121.5	121.5	0.0	−1.3	−114.49933	0.0002

For every pair of rows the first line represents a point along the IRC path and the second line represents a point at which the 12 secondary coordinates have been optimized for the given values of Φ, δ_1, δ_2

Row labels: C = cyclopropylidene; A = allene; T = transition state (internal coordinates interpolated according to Sect. 5.2)

Column labels:

$r_{01} = C_0$–C_1 stretch $r_{11'} = C_1$–$H_{1'}$ stretch $\alpha_{011} = C_0$–C_1–H_1 bend $\alpha_{022'} = C_0$–C_2–$H_{2'}$ bend

$r_{02} = C_0$–C_2 stretch $r_{22} = C_2$–H_2 stretch $\alpha_{011'} = C_0$–C_1–$H_{1'}$ bend $\beta_1 = C_0$–($C_1H_1H_{1'}$) out of plane bend

$r_{11} = C_1$–H_1 stretch $r_{22'} = C_2$–$C_{2'}$ stretch $\alpha_{022} = C_0$–C_2–H_2 bend $\beta_2 = C_0$–($C_2H_2H_{2'}$) out of plane bend

r in bohr; α, β, δ, Φ in degrees; energy in hartree; Max.grad = largest component of the gradient with respect to the 12 optimized coordinates (convergence criterion: Max.grad $\leqslant 0.0005$)

twelve secondary coordinates do yield the optimized energy for the listed (Φ, δ_1, δ_2) values.) A comparison of the two rows for each pair shows that, for all practical intents and purposes, the intrinsic reaction path can be considered to lie on the surface $E(\Phi, \delta_1, \delta_2)$ which is determined by minimizing E with respect to the twelve secondary coordinates, as outlined in the preceding section.

The energy along the intrinsic reaction path is plotted in Fig. 6 (top). It exhibits the transition state at $\Phi = 84.2°$ with an activation energy of 40 kcal/mol. In the third paper [73] we shall see that deployment of an extended basis hardly changes the transition state geometry, but yields a considerably lower barrier. For the ascending part of the reaction path the figure also shows that variation of the energy with Φ which results when the energy is minimized for Φ = constant. This curve is extended to $\Phi = 50°$ in order to show that there exists indeed a minimum, i.e., a (meta)stable species at $\Phi = 59.5°$. On the

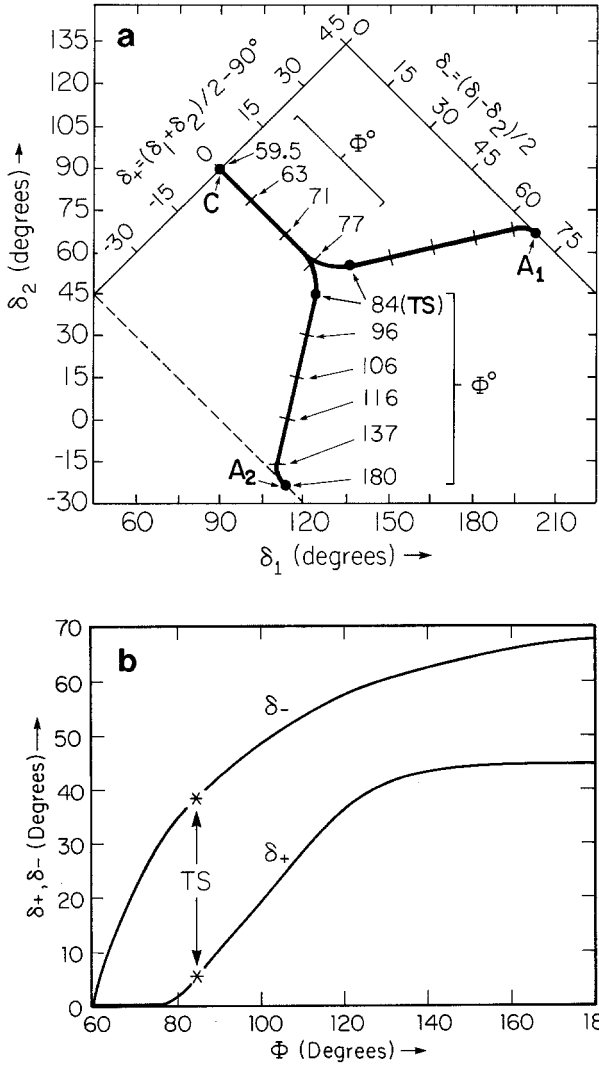

Fig. 5a,b. Intrinsic reaction path in the Φ, δ_1, δ_2 space. **a** Projection in the δ_1, δ_2 plane. The Φ values are indicated for various points. Also shown are the coordinates δ_+, δ_-. **b** Variation of δ_+, δ_- with Φ along one of the reaction paths

descending part of the path beyond the transition state, minimization for constant Φ does not yield a corresponding curve as we shall see.

Figure 6 (top) also provides a unifying color key for identifying the various energy ranges on the subsequent figures. On these figures, contours are drawn at 10 mhartree ($\sim$6 kcal/mol) increments, corresponding to the horizontal lines on Fig. 6 (top) and the areas between the contours are filled in by the same colors as those in Fig. 6 (top). In this manner it is possible *to compare energies on different contour maps*. Areas with energies higher than those depicted in red are colored grey as also indicated in Fig. 6 (top).

4. The reaction surface $E(\Phi, \delta_1, \delta_2)$

The variation of the energy along the reaction path provides only an incomplete picture of the reaction. Indeed, it will be seen that the reaction path picture suggested by Fig. 5 is particularly inadequate beyond the transition state. To obtain a fuller insight it is necessary to examine slices through the energy surface $E(\Phi, \delta_1, \delta_2)$ for various values $\Phi =$ constant as discussed in Sect. 2.3. The resulting contour maps $E(\delta_1, \delta_2)$ are displayed in Figs. 6 (bottom) to 15.

$\Phi = 59.5°$, cyclopropylidene: Fig. 6 (bottom). By means of a geometry optimization involving all 15 internal coordinates the minimum representing the reactant was found to have a Φ angle of 59.5°. There is no physical difference between the four equivalent minima denoted by m at the positions $(\delta_1 = 90°, \delta_2 = 90°)$, $(\delta_1 = 90°, \delta_2 = -90°)$, $(\delta_1 = -90°, \delta_2 = -90°)$, $(\delta_1 = -90°, \delta_2 = 90°)$, all of which correspond to the two CH_2 planes being exactly perpendicular to the C–C–C plane. We shall follow only the reaction of the species which is situated at $(\delta_1 = 90°, \delta_2 = 90°)$.

The maximum (M) occurs for $(\delta_1 = 0°, \delta_2 = 0°)$, corresponding to the two CH_2 planes lying flat in the CCC plane, causing maximal steric hindrance of the hydrogens.

$\Phi = 50°$. This panel, which is not displayed, was calculated as an aid to interpolation beyond the cyclopropylidene minimum. Its basic characteristics are the same as those of the preceding panel, except that all energies are considerably higher (about 30 mhartree at the minimum).

$\Phi = 70°$: Fig. 7 (top). The minimum m is still located at $(\delta_1 = 90°, \delta_2 = 90°)$. Its energy has increased by about 20–30 mhartree. Moreover the area around the minimum is elongated, giving the CH_2 planes a greater ease for rotational motion. We recall (see Fig. 4) that a progression on the surface in the direction of the elongation of the minimum valley, i.e., along the line $\delta_1 + \delta_2 = 180°$, corresponds to the *disrotatory* rotation of the two CH_2 groups. The direction perpendicular to it, i.e., along the line $\delta_1 - \delta_2 =$ constant, corresponds to the *conrotatory* rotation of the CH_2 groups. The maximum is no longer at $(\delta_1 = 0°, \delta_2 = 0°)$. It has separated in two (M_1 and M_2) along a conrotatory deformation and a saddle point has developed at $(\delta_1 = 0°, \delta_2 = 0°)$.

$\Phi = 75°$: Fig. 7 (bottom). The difference between this panel and the preceding one is that there is now much less variation in energy between the various parts of the entire panel. The minimum area around m is elongated further. The two maxima M_1 and M_2 have moved farther apart. In fact, the minimum valley seems sandwiched between two maxima (M_2 and M_3). The saddle point at the

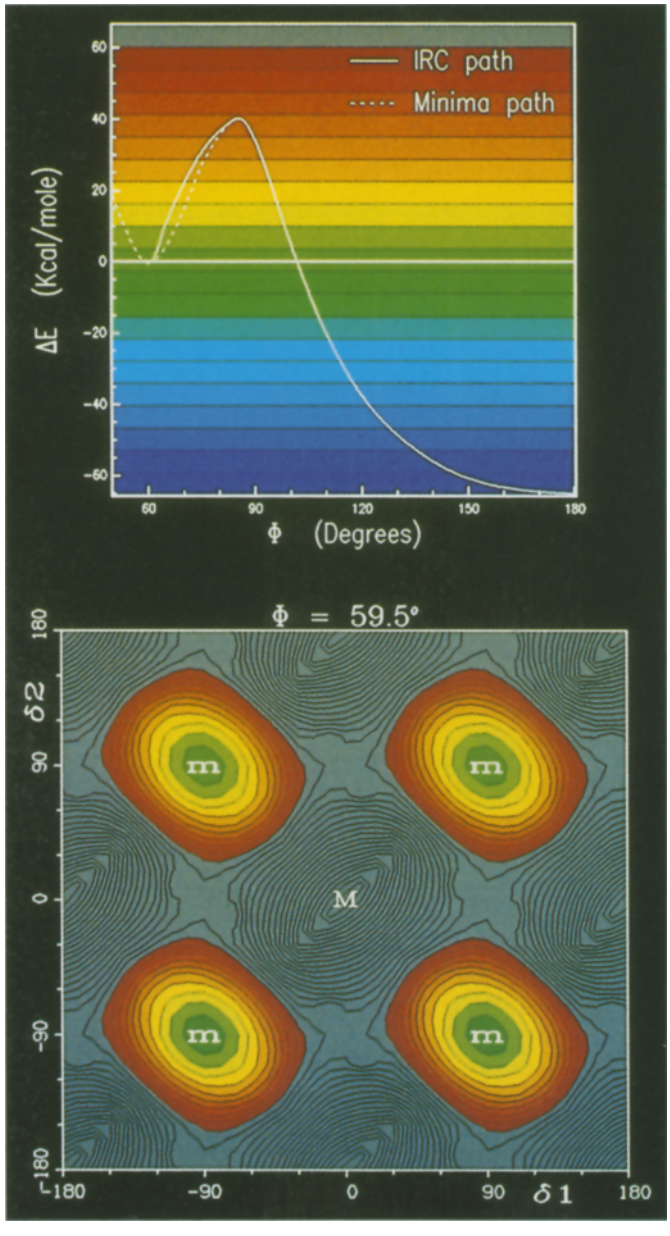

Fig. 6. *(top)*: reaction energy as function of the ring opening angle Φ. Increments between contours = 10 millihartree. *Bottom*: Contours of $E(\Phi, \delta, \delta_1)$ for $\Phi = 59.5°$. *Color key*: See end of Sect. 3 and **Fig. 6.** *(top)*

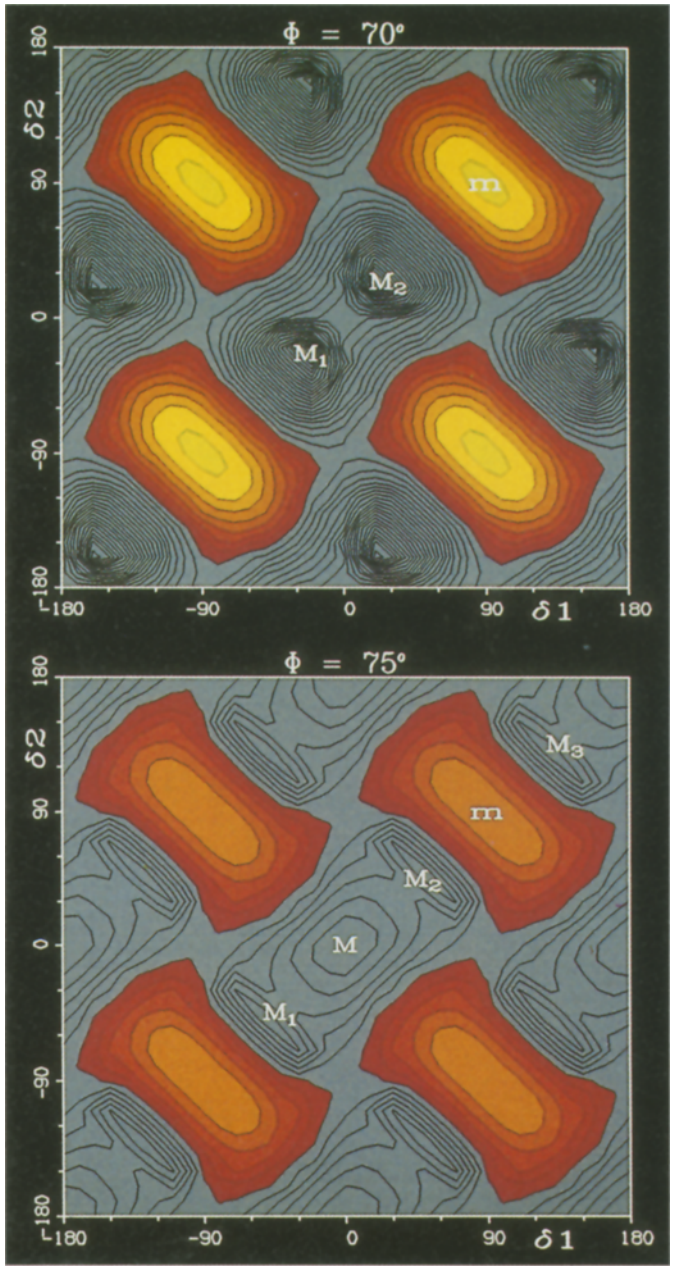

Fig. 7. Contours of $E(\Phi, \delta_1, \delta_1)$ for $\Phi = 70°$ (*top*) and for $\Phi = 75°$ (*bottom*). *Color key*: See end of Sect. 3 and Fig. 6 (top)

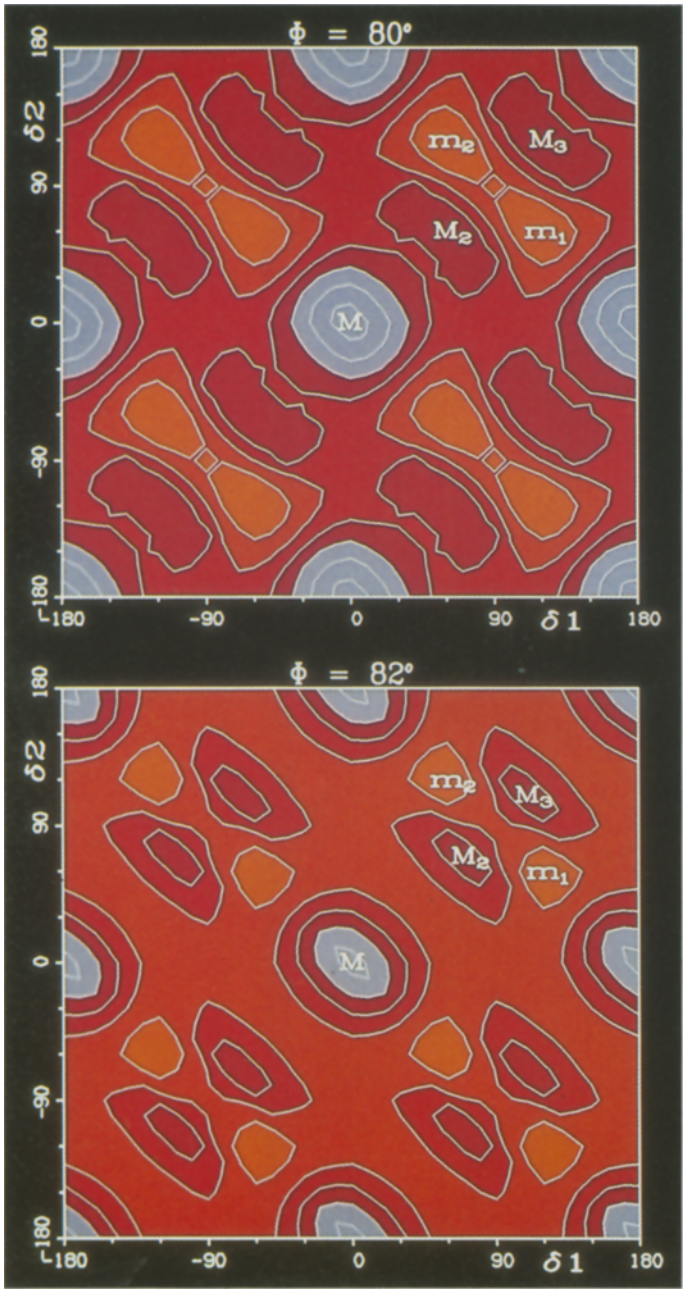

Fig. 8. Contours of $E(\Phi, \delta_1, \delta_1)$ for $\Phi = 80°$ (*top*) and $\Phi = 82°$ (*bottom*). *Color key*: See end of Sect. 3 and Fig. 6 (top)

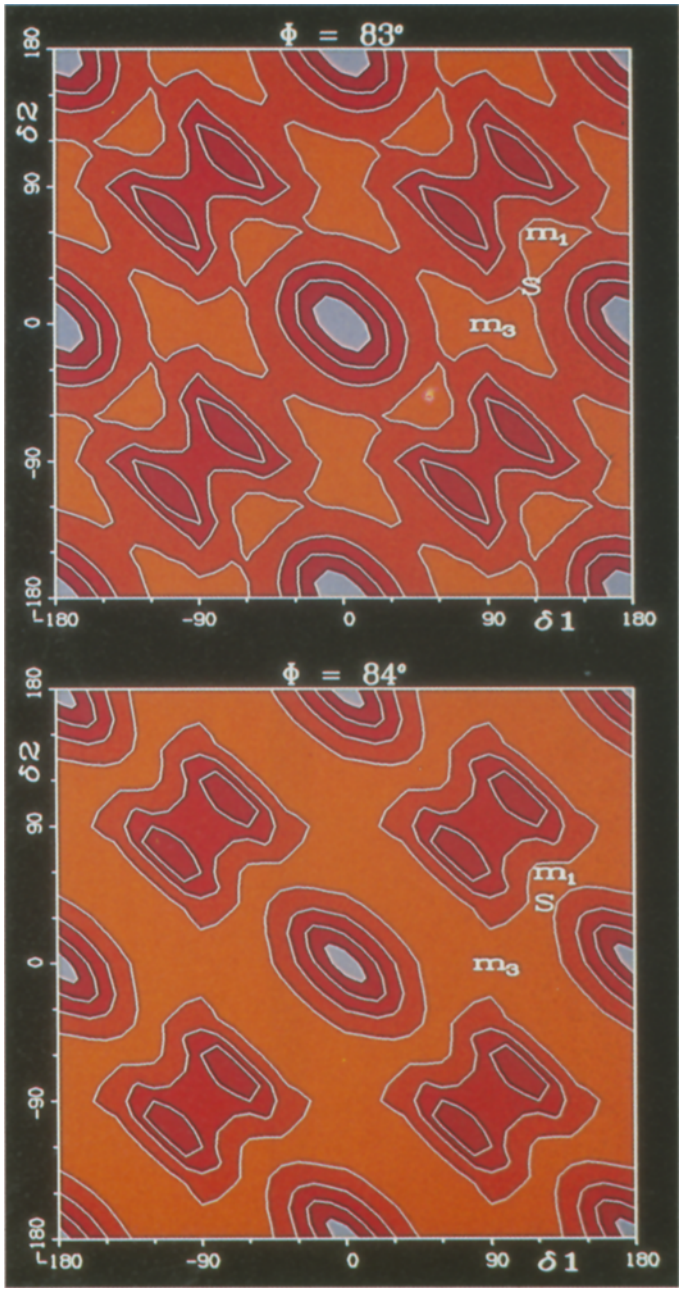

Fig. 9. Contours of $E(\Phi, \delta_1, \delta_1)$ for $\Phi = 83°$ (*top*) and for $\Phi = 84°$ (*bottom*). *Color key*: See end of Sect. 3 and Fig. 6 (top)

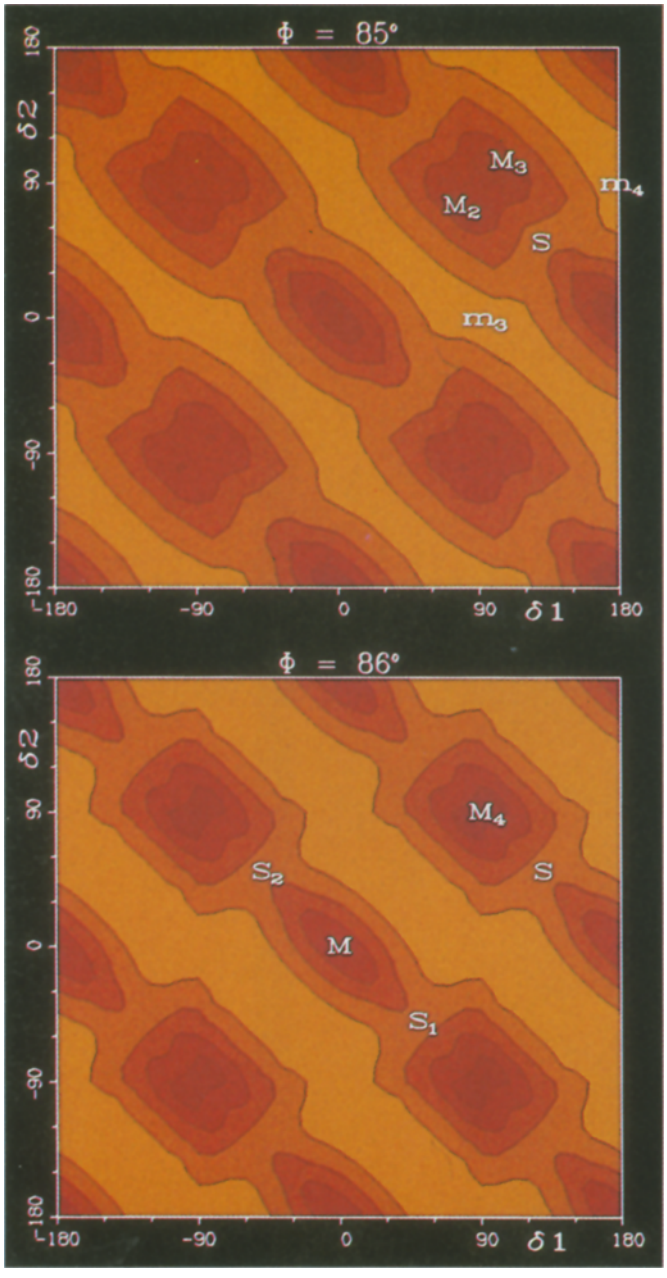

Fig. 10. Contours of $E(\Phi, \delta_1, \delta_1)$ for $\Phi = 85°$ (*top*) and for $\Phi = 86°$ (*bottom*). *Color key*: See end of Sect. 3 and Fig. 6 (top)

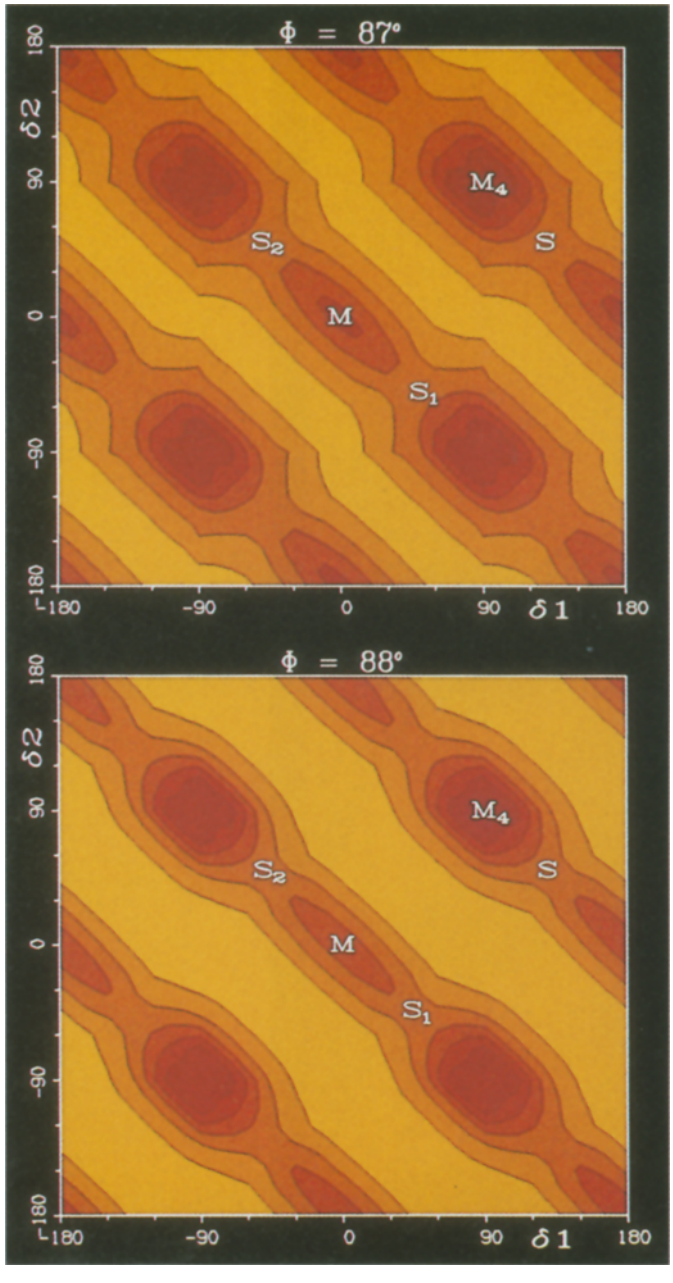

Fig. 11. Contours of $E(\Phi, \delta_1, \delta_1)$ for $\Phi = 87°$ (*top*) and for $\Phi = 88°$ (*bottom*). *Color key*: See end of Sect. 3 and Fig. 6 (top)

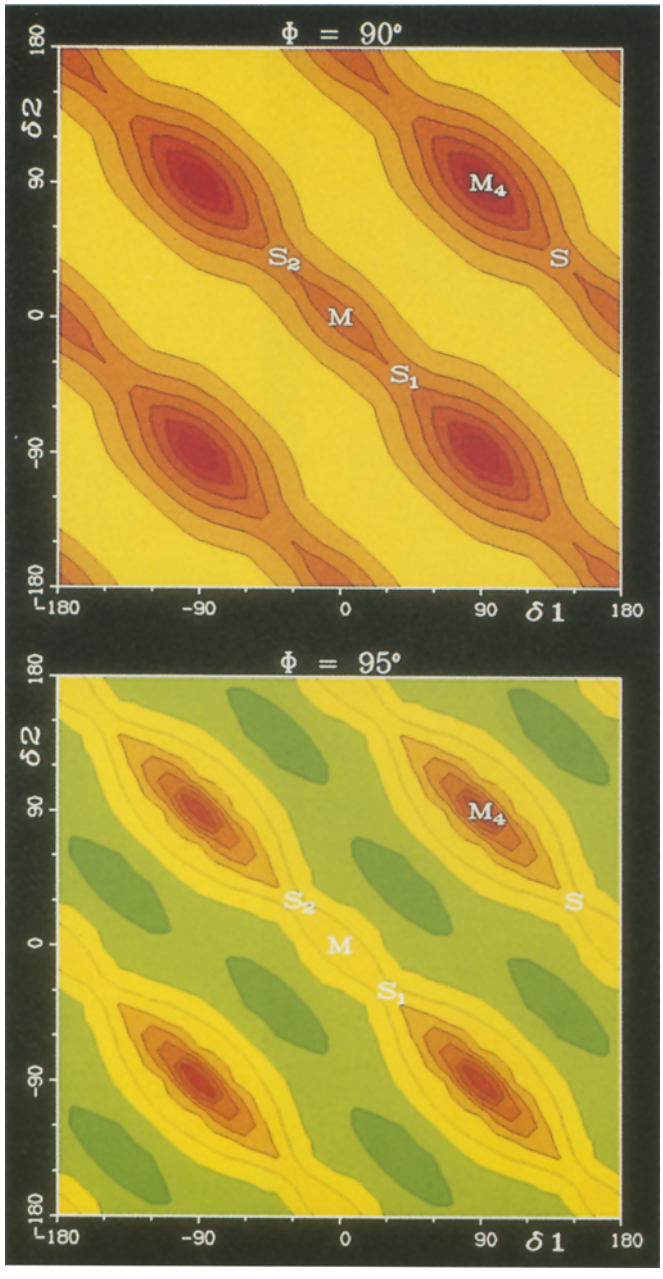

Fig. 12. Contours of $E(\Phi, \delta_1, \delta_1)$ for $\Phi = 90°$ (*top*) and for $\Phi = 95°$ (*bottom*). *Color key*: See end of Sect. 3 and Fig. 6 (top)

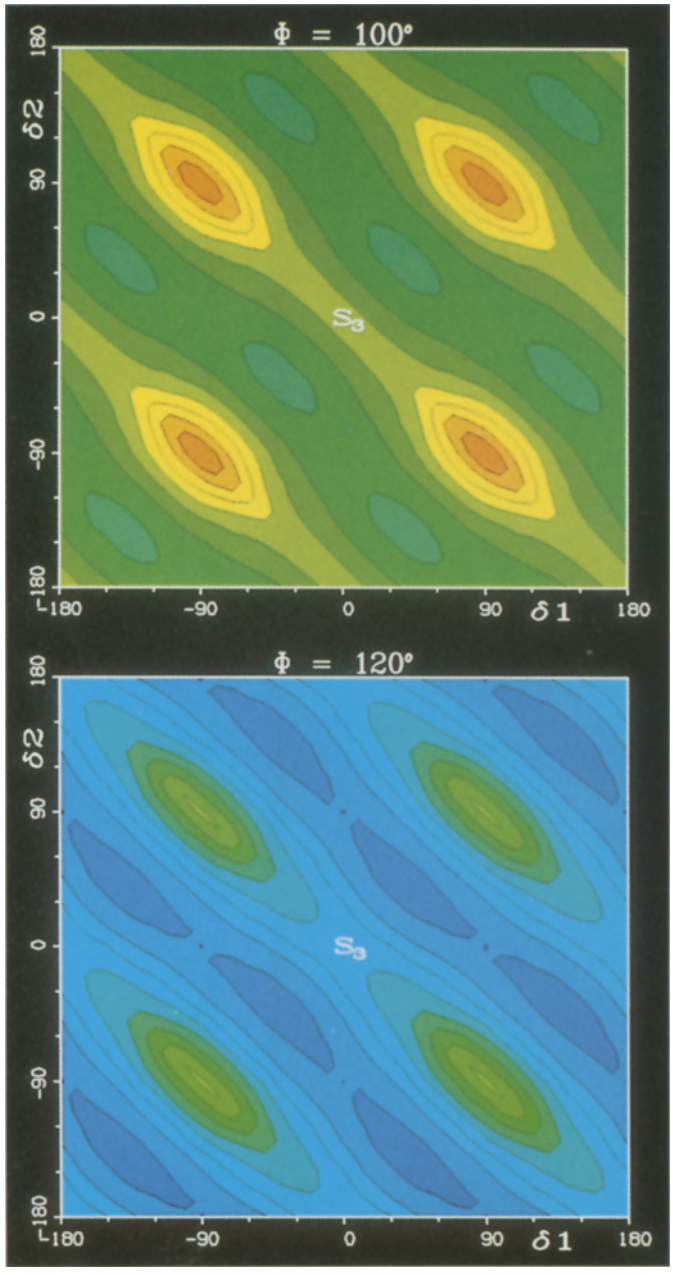

Fig. 13. Contours of $E(\Phi, \delta_1, \delta_1)$ for $\Phi = 100°$ (*top*) and for $\Phi = 120°$ (*bottom*). *Color key*: See end of Sect. 3 and Fig. 6 (top)

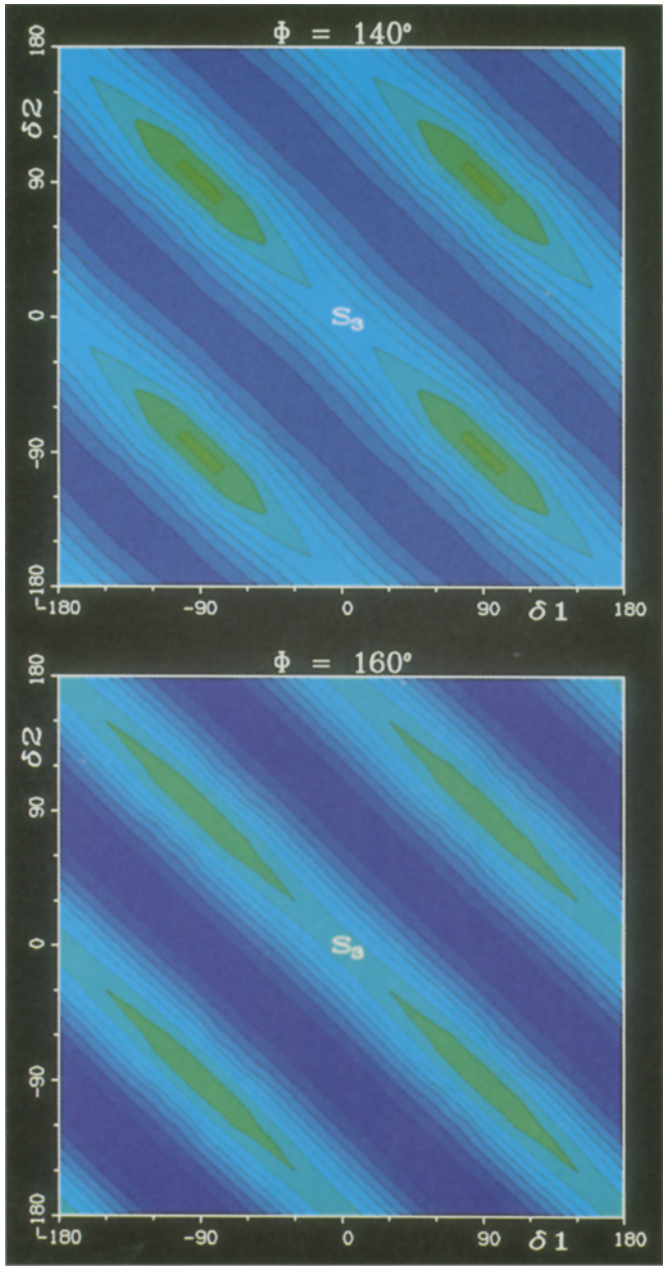

Fig. 14. Contours of $E(\Phi, \delta_1, \delta_1)$ for $\Phi = 140°$ (*top*) and for $\Phi = 160°$ (*bottom*). *Color key*: See end of Sect. 3 and Fig. 6 (top)

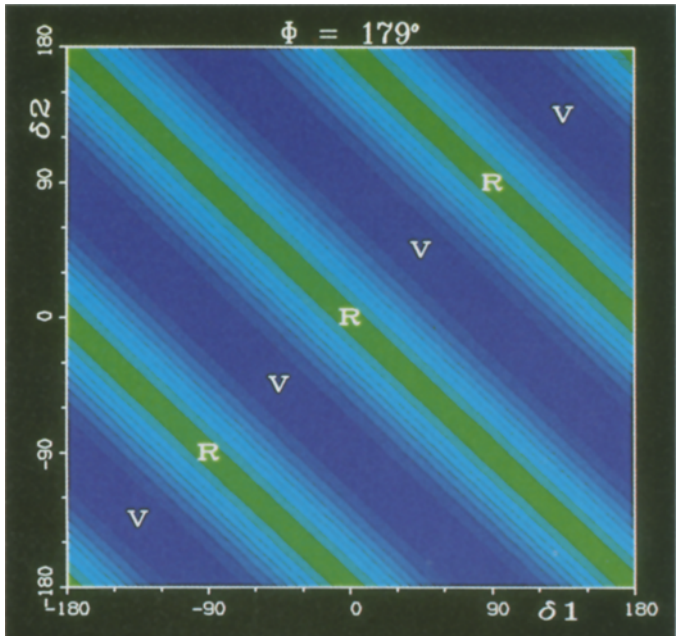

15

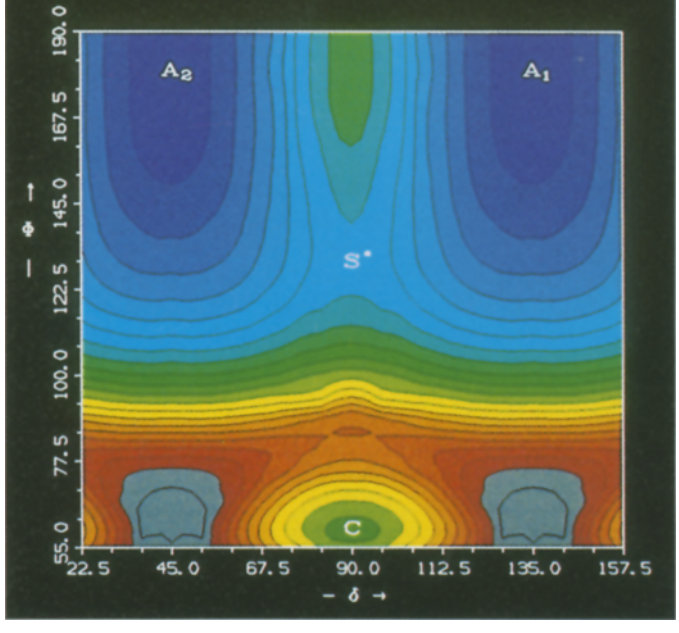

16

Fig. 15. Contours of $E(\Phi, \delta_1, \delta_1)$ for $\Phi = 179°$. *Color key*: See end of Sect. 3 and Fig. 6 (top)

Fig. 16. Contours of $E(\Phi, \delta)$ where $\delta = (\delta_1 + \delta_2)/2$. Cyclopropylidene: C. allene: A_1, A_2; allene isomerization saddle: S*. *Color key*: See end of Sect. 3 and Fig. 6 (top)

origin has split into two and a new maximum, denoted again by M, is rising up at ($\delta_1 = 0°$, $\delta_2 = 0°$).

$\Phi = 80°$: Fig. 8 (top). The essential difference from the previous panels is that the minimum has now separated in two (m_1 and m_2), as if the two maxima M_2 and M_3 had squeezed the minimum valley on either side. This split in two minima implies a disrotatory motion of the CH_2 groups as the Φ angle opens and the molecule moves towards the transition state. We are seeing the *first bifurcation* in the reaction path, corresponding to two alternative motions: Either the top two hydrogens come closer together and the two bottom ones move farther apart or vice versa. This bifurcation is associated with the reduction of symmetry from C_{2v} to C_s. If one draws the contours of E in the plane $\delta_1 + \delta_2 = 180°$ with the coordinate axes Φ and $\delta_- = (\delta_1 - \delta_2)/2$, then one sees that the *orthogonal trajectories* of these contours start to bifurcate *right away* at the minimum $\Phi = 59.5°$. For reasons of simplicity, we shall limit our discussion to only one of the two cases, namely the path moving to the right, corresponding to m_1. The value of the minimum has further increased.

$\Phi = 82°$: Fig. 8 (bottom). This panel is a further evolution from the previous one. The minima m_1 and m_2 on the disrotatory line $\delta_1 + \delta_2 = 180°$ are more distinctly separated. The maxima M_2 and M_3 along the conrotatory line $\delta_1 - \delta_2 = 0$ are getting closer together, converging on the point ($\delta_1 = 90°$, $\delta_2 = 90°$).

$\Phi = 83°$: Fig. 9 (top). Except for the fact that the minimum m_1 has moved further along the disrotatory motion path, corresponding to a further C_s-preserving inclination of the CH_2 planes, the important feature is the appearance of a new minimum (m_3) at around ($\delta_1 = 90°$, $\delta_2 = 0°$). A little reflection shows that this second minimum is the one corresponding to the relative positions which the two CH_2 planes will have in allene when Φ becomes 180°. An energy barrier, denoted as the saddle point S, separates the two minima m_1 and m_3. The new minimum m_3 is higher by about 6 kcal/mol than m_1. The latter has again increased in energy.

$\Phi = 84°$: Fig. 9 (bottom). This panel differs from the one for $\Phi = 83°$, in that the new minimum m_3 near ($\delta_1 = 90°$, $\delta_2 = 0°$) is now *lower* in energy than the original one (m_1) on the line $\delta_1 + \delta_2 = 180°$. There still exists a saddle point (S) between the two. For fixed Φ, the system would therefore stay at the original minimum m_1. The saddle S has, however, moved quite close to m_1.

Of particular interest is the fact that the new minimum m_3 is extremely shallow in the disrotatory direction. There really exists a low-lying valley along the line $\delta_1 + \delta_2 = 90°$. Motions along this line correspond to *disrotatory synchronized* rotations of the two CH_2 planes, with a phase lag of 90°, as was illustrated earlier on line 2 of Fig. 4. It represents a cogwheel-type motion of the two CH_2 groups *which preserves chirality* (if one distinguishes the H atoms by their numbering). For $\Phi = 84°$ there clearly exists very little resistance against such coupled rotations.

$\Phi = 85°$: Fig. 10 (top). There is no longer a minimum on the line $\delta_1 + \delta_2 = 180°$. Instead, the minimum m_1 of the preceding panel has now turned into a saddle point (S). This saddle has come about through the merging of the two saddle points which, in the preceding panel, were located on either side of what was there the minimum m_1. The molecule is now free to slide down to the new minimum, i.e., it has passed the transition state.

At this stage we note that there are, in fact, two valleys on Fig. 10, one on each side of the saddle S. They contain the minima m_3 and m_4, respectively, and *correspond to two sets of geometries which are each others' stereoisomeric, chiral images*. It is evident that the system can descend from the saddle point S in either direction and we therefore have a *second bifurcation* on the reaction path. It is associated with the further reduction in symmetry from C_s to C_1. It is also apparent that the highest point on the reaction path, i.e., the transition state, must occur between $\Phi = 84°$ and 85°. We shall examine the detailed shape of the energy surface in this neighborhood in Sect. 6.1.

Finally, it may be noted that the maxima M_2 and M_3 converge on a point near ($\delta_1 \doteq 90°$, $\delta_2 = 90°$) and have almost merged into one.

$\Phi = 86°$ to 95°: Fig. 10 (bottom) to Fig. 12 (bottom). The previous maxima M_2 and M_3 have now merged into one maximum (M_4) near ($\delta_1 = 90°$, $\delta_2 = 90°$). The saddle points such as S, S_1, and S_2 now lie on the lines $\delta_1 + \delta_2 = 180°$ or 0°, i.e., the disrotatory lines on which the original minima used to lie. As Φ increases, the saddles S_1 and S_2 approach the maximum M at the origin from both sides, with M becoming less pronounced.

The entire surface is getting progressively lower in energy as Φ opens from 85° to 95° and the reaction path is on its way downhill way into the valley towards the product. However, it stands to reason that *the free disrotatory cogwheel motions along the isoenergetic valleys can mix unpredictably with the conrotatory downhill motion*. Therefore there will not really exist a well-defined unique reaction path from the transition state to the product.

$\Phi = 100°$ to 160°: Figs. 13 and 14. The entire panel is drastically decreasing in energy. There are two notable features compared to the previous panels:

(i) The low-lying valleys corresponding to $\delta_1 + \delta_2 = \pm 90°$ (disrotatory, cogwheel-like, of Fig. 4) become straighter and flatter so that the cogwheel-like rotations of the two CH_2 groups become freer and freer and the downhill reaction path less and less clearly defined. It should be noted that *each point in each valley* $\delta_1 + \delta_2 = \pm 90°$ will go over into *staggered* (D_{2d}) allene if the angle Φ is opened up to 180° without changing δ_1 and δ_2, (i.e., in a nonrotatory fashion) while the remaining 12 coordinates go over into the allene values.

(ii) The two saddle points S_1 and S_2 from Fig. 12 have come together and coalesced at the point ($\delta_1 = 0°$, $\delta_2 = 0°$) and the equivalent point ($\delta_1 = 180°$, $\delta_2 = 0°$) where the maximum M was in Fig. 12 (top), so that we now have saddles (S_3) at these points. As Φ increases, the energy of this saddle first decreases and then increases; it has its lowest value for $\Phi \simeq 133°$. This point ($\Phi = 133°$, $\delta_1 = 180°$, $\delta_2 = 0°$) corresponds to both CH_2 groups lying *in* the CCC plane and, in the next section, it will be seen that it represents the transition state for the isomerization reaction path between the two stereoisomeric allene products. It is apparent that this allene isomerization transition state, the reactant ($\Phi = 60°$, $\delta_1 = \delta_2 = 90°$) as well as the average geometry ($\Phi = 84°$, $\delta_1 = 129°$, $\delta_2 = 51°$) of the two ring-opening transition states all have the same C_s symmetry plane. The three geometries are connected by the disrotatory C_s-preserving pathway $\delta_1 + \delta_2 = 180°$ shown at the top of Fig. 4.

In the subsequent two papers [73, 74] it will be seen that the wavefunctions of the reactant and the average ring-opening TS belong to the irreducible representation A′ of the group C_s, whereas that of the allene isomerization TS belongs to A″. It follows that, along the C_s-preserving path $\delta_1 + \delta_2 = 180°$, there

exist two states with symmetries $^1A'$ and $^1A''$, respectively, which cross between $\Phi = 86°$ and 133°. In the third paper [73] this crossing is found to occur at about ($\Phi = 100.3°$, $\delta_1 = 25.6°$, $\delta_2 = 154.4°$). At this point the global surface discussed in the present paper has therefore a *conical intersection* with a higher-lying surface.

$\Phi = 179°$, allene: Fig. 15. The calculations were performed for $\Phi = 179°$ instead of 180° so that the same computer program could be used, which was contingent upon being able to define the CCC plane. The contours are a series of perfectly straight valleys and ridges implying completely uninhibited motions along lines $\delta_1 + \delta_2 =$ constant. The valleys (V) correspond to the staggered (D_{2d}) configuration of allene and the ridges (R) to the eclipsed (D_{2h}) configuration. This result is easy to understand, because motions along the valleys and ridges correspond to *rigid rotations* of the molecule about the linear CCC axis. This means that for $\Phi = 180°$, the average $(\delta_1 + \delta_2)/2$ ceases to be an internal coordinate, so that motions in this direction are indeed free.

5. The energy as a function of Φ and $\delta = (\delta_1 + \delta_2)/2$

Whereas the plot given in Fig. 5a shows the variation of the energy along the intrinsic reaction coordinate, the plots in Figs. 5b to 15 exhibit the variation of the molecular energy with all three reaction coordinates Φ, δ_1, δ_2. While the latter representation is required for providing complete information about the rotations of the hydrogens, it makes it more difficult to visualize the reaction path in its entirety. It is therefore useful to consider an intermediate representation, namely to examine the energy as a function of Φ and the "*average conrotatory rotation angle*" $\delta = (\delta_1 + \delta_2)/2$ which is related to the coordinate δ_+ introduced in Sect. 3 and Fig. 5. These energy values were obtained by finding, for each panel $\Phi =$ constant and *on each line* $\delta_1 + \delta_2 =$ constant, the energy minimum with respect to the "disrotatory variable" $\delta_- = (\delta_1 - \delta_2)/2$. The new independent variable δ shows how far off the C_s symmetry line ($\delta = 90°$) the molecule is. Although there are now 13 optimized internal coordinates and only two independently varying ones, the new surface could hardly have been generated without first generating the larger surface in terms of $(\Phi, \delta_1, \delta_2)$, because the appropriate choice of two reduced coordinates can be justified only after studying the preceding results.

Contours of this intermediate reaction surface are displayed in Fig. 16. The contour increments and the color scheme are the same as before. The average conrotatory dihedral angle δ is the horizontal axis and the ring-opening angle Φ is the vertical axis. The reactant, cyclopropylidene, is at the minimum for ($\delta = 90°$, $\Phi = 59.5°$) and denoted by C. As the reaction proceeds, the molecule moves upwards on the map, in the direction of increasing Φ. It should be noted that the $\delta = 90°$ line embodies *both, nonrotatory or disrotatory* behavior of the CH_2 planes in such a way that the molecule retains C_s symmetry. Deviations from this line imply a breaking of the C_s symmetry, and can represent mixtures of conrotatory, monorotatory, or asymmetric disrotatory motion of the CH_2 planes.

Starting at C, the floor of the valley in which the molecule is advancing starts to rise. At a Φ angle of about 84.5° there occurs a maximum on the $\delta = 90°$ line and shortly before reaching this maximum, the $\delta = 90°$ line changes from a valley into a ridge. This happens at a "valley-ridge inflection point" [69]. The

presence of the ridge is expected to cause the molecule to fall away from the C_s symmetry line and to move over one or the other of the two saddle points situated on either side towards one or the other of the two allene product minima A_1 and A_2. There is no reason why the molecule would move in one direction rather than in the other, i.e., towards one allene stereoisomer rather than to the other, so that we have the conditions for a non-preferential bifurcation. From the results described in Sect. 3 it is apparent that the reaction path first follows the line $\delta = 90°$ from cyclopropylidene to about 80°, i.e., shortly before the maximum at $\Phi = 84.5°$. It then branches, goes over one or the other of the two transition states and descends to A_1 or A_2. Thus, *the bifurcation occurs in the vicinity of the transition states* and the point on the $\delta = 90°$ axis halfway between the two transition states is practically isoenergetic with them. The maximum on the $\delta = 90°$ axis lies about 0.2 kcal/mol higher. It was shown in Sect. 3 that the steepest descent lines from the transition state to the *reactant* (C) approach the axis $\delta = 90°$ very quickly.

In a previous publication [69] we have given an in-depth analysis of the general features that are associated with bifurcations which occur when a reaction path on an energy surface in a two-dimensional parameter space branches towards two products under loss of C_s symmetry. In that analysis the valley-ridge inflection point plays an essential role. There, we have also discussed in greater detail the surface depicted in Fig. 16 in terms of the general theory and shown that it displays a *bifurcating transition region* of a type called there "Case 3b".

The reduced reaction surface of Fig. 16 also exhibits the pathway for the *internal isomerization of allene* by a relative rotation of the two CH_2 groups with respect to each other. It is apparent that this path leads from one allene, A_1 say, over the saddle S* to the other allene, say A_2. Such a reaction path manifestly implies a concerted twisting and bending motion. This conclusion is illustrated in more detail in the preceding $\Phi =$ constant contour panels. For $\Phi = 179°$ (Fig. 15), one finds that, between the valleys $\delta_1 + \delta_2 = 90°$ and $\delta_1 + \delta_2 = -90°$ (corresponding to the two isomers), there exists a barrier of about 90 mhartree (55 kcal/mol). However, for $\Phi = 140°$ (Fig. 14, top) one sees that, at its lowest point, i.e., at the saddle point S_3, the isomerization barrier has only a value of about 70 mhartree (44 kcal/mol). It is therefore energetically advantageous for allene to bend before twisting the two CH_2 groups with respect to each other. The exact location of this transition state was determined by an unrestricted saddle point optimization [12] which yielded the bending angle $\Phi = 133.3°$ ($\delta_1 = 180°, \delta_2 = 0°$) and a barrier of about 42 kcal/mol. As discussed in the preceding section for Figs. 13 and 14, there occurs a change from A′ to A″ symmetry along the C_s-preserving path $\delta = 90°$ at $\Phi = 100.3°$ (see point CR in Fig. 3 of ref. 73). At this point, the surface shown in Fig. 16 has therefore a conical intersection with a higher-lying surface even though it varies quite gradually in that region.

6. The bifurcating transition region

6.1. Detailed structure on the surface $E(\Phi, \delta_1, \delta_2)$

While it is fairly straightforward to recognize the bifurcation in the two-dimensional representation of Fig. 16, it is more difficult to visualize it on the full energy surface in terms of all three variables Φ, δ_1, δ_2, and we therefore

glossed over this point in the discussion of the $\Phi = 85°$ panel (Fig. 10). For an effective analysis of this matter it is useful to express the energy in terms of the average conrotatory and disrotatory angles $\delta_+ = (\delta_1 + \delta_2)/2 - 90°$ and $\delta_- = (\delta_1 - \delta_2)/2$, which were introduced at the end of Sect. 2.3. We recall that a variation of δ_+, with δ_- being held fixed, represents a conrotatory motion with a phase lag of δ_-, whereas a variation of δ_-, with δ_+ being held fixed, describes a disrotatory motion with a phase lag of δ_+.

From the discussion in connection with Fig. 3 and from the panels of Figs. 6 (bottom)–15 it is apparent that the energy must be an *even* function of δ_+ so that we have

$$E = F(\delta_+^2, \delta_-, \Phi).$$

In order to discuss the behavior of this function in the region of interest, we follow an approach similar to that used in our bifurcation analysis of [69]. About 200 energy values at points in the domain:

$$-12.5° \leqslant \delta_+ \leqslant 12.5°, \qquad 27.5° \leqslant \delta_- \leqslant 52.5°, \qquad 82° \leqslant \Phi \leqslant 86°$$

spaced at increments:

$$\Delta\delta_+ = 5°, \qquad \Delta\delta_- = 5°, \qquad \Delta\Phi = 1°$$

were used to determine a least-mean-square fit of the energy to the polynomial:

$$F = a_0 + b_1\delta_+^2 + b_2\delta_- + b_3\Phi + (c_1\delta_+^4 + c_2\delta_-^2 + c_3\Phi^2 + 2c_{12}\delta_+^2\delta_- + 2c_{13}\delta_+^2\Phi + 2c_{23}\delta_-\Phi)/2$$

which represents a second-order expansion in terms of the variables $\delta_+^2, \delta_-, \Phi$. This fit yields the following coefficient values

$$a_0 = -115546.7054$$

$$b_1 = 1.152513, \qquad b_2 = 8.363468, \qquad b_3 = 24.48725$$

$$c_1 = -0.00000371, \qquad c_2 = 0.05786903, \qquad c_3 = -0.22787172$$

$$c_{12} = -0.00273508, \qquad c_{13} = -0.01241789, \qquad c_{23} = -0.12481562$$

where the angles are expressed in degrees and the energy in mhartree. The numbers of decimals are chosen so as to yield the polynomial F accurate to 1 microhartree which, although physically meaningless, is needed to exhibit the topographical details of F in this region. The accuracy of the fit is measured by the ratio of the mean-square deviation to the average variation of the energy over the region covered. It is about 0.04 which shows that the representation is germane and good. With this polynomial we are in a position to discuss the behavior of the energy surface in the flat bifurcating transition region.

Figure 17 exhibits contours of the polynomial F which are entirely analogous to those of Figs. 6 (bottom)–15. As before, each panel corresponds to a fixed value of Φ = constant. The vertical line $\delta_+ = 0$ corresponds to the diagonal line $\delta_1 + \delta_2 = 180°$ on the previous panels and the horizontals δ_- = constant correspond to diagonals $\delta_1 - \delta_2$ = constant on the previous panels. Figure 17 displays eight panels corresponding to values of Φ from 84° to 86°. They furnish a detailed close-up of the energy surface in this neighborhood between the previous panels of Figs. 9 and 10. The labels m_1 and S in Fig. 17 denote exactly the same minima and saddle points as they did on Figs. 9 and 10.

The approximately semicircular regions containing the minima m_1 represent cross sections through a tube, extending in the Φ direction, which is essentially the entrance channel. The tube has two edges and the saddle points S, S* lie along these edges. With increasing Φ values the tube cross section becomes smaller and smaller, and the two edges move closer together. For $\Phi = 84.500207°$ the saddles S and the minimum m_1 coalesce into what is now a saddle point and no more a minimum on the line $\delta_+ = 0$. At this point the tube cross section has shrunk to zero so that the entrance channel terminates. The exact location of the coalescence point is given by the equations:

$$\delta_+ = 0, \qquad (\partial F/\partial \delta_-) = 0, \qquad \partial^2 F/(\partial \delta_+)^2 = \partial F/\partial(\delta_+^2) = 0.$$

This point is the *generalization of the valley-ridge inflection point* discussed in [69] for two-dimensional surfaces. Its existence is an *essential element of the bifurcation* as explained there. Since it occurs for a Φ value which is larger than that of the transition states, it has to be classified as a "Case (3c) close to Case (3b)" in terms of the analysis in [69].

From the polynomial F one furthermore readily deduces the *exact transition states of the ring opening*, because they satisfy the three equations:

$$(\partial E/\partial \delta_+) = (b_1 + c_1 \delta_+^2 + c_{12}\delta_- + c_{13}\Phi)2\delta_+ = 0,$$
$$(\partial E/\partial \delta_-) = b_2 + c_2 \delta_- + c_{12}\delta_+^2 + c_{23}\Phi = 0,$$
$$(\partial E/\partial \Phi) = b_3 + c_3 \Phi + c_{13}\delta_+^2 + c_{23}\delta_- = 0.$$

It is readily verified that the transition states have $\delta_+ \neq 0$ so that the first equation can be replaced by

$$b_1 + c_1 \delta_+^2 + c_{12}\delta_- + c_{13}\Phi = 0$$

which together with the second and third, yields for the transition states the angles:

$$\delta_+ = \pm 5.946257°, \qquad \delta_- = 38.848835°, \qquad \Phi = 84.243506°.$$

They are the two saddle points denoted by S*, which are shown on the panel for this value of Φ. The transition state energy is -114.332535 hartree which differs from the coalescence point energy, namely -114.332468 hartree, by only 0.04 kcal/mol. There is a third solution to the equations $(\partial E/\partial \delta_+) = (\partial E/\partial \delta_-) = (\partial E/\partial \Phi) = 0$, given by $\delta_+ = 0$ and the equations:

$$b_2 + c_2 \delta_- + c_{23}\Phi = 0,$$
$$b_3 + c_3 \Phi + c_{23}\delta_- = 0.$$

It is

$$\delta_+ = 0°, \qquad \delta_- = 39.987908°, \qquad \Phi = 85.546421°,$$

and denoted by S* on Fig. 17. It is found to be a saddle with two negative eigenvalues, one in the δ_+ direction, the other in the Φ direction. It is readily confirmed that at this point the function $\tilde{E}(\Phi)$ has a *maximum*, where $\tilde{E}(\Phi)$ is defined as the *minimum of E, with respect to* δ_-, *on the line* $\delta_+ = 0$, *for a given value* Φ = *constant*, i.e., $\tilde{E}(\Phi)$ is the value at the points which were denoted by m_1 on the various panels of Figs. 9 and 17. This maximum of $\tilde{E}(\Phi)$ is -114.332196 hartree and lies only 0.2 kcal/mol higher than the transition state. The existence of such a maximum is *a necessary concomitant surface feature when the bifurcation occurs before the transition state*, as shown for "cases 3a, 3b, 3c" in [69].

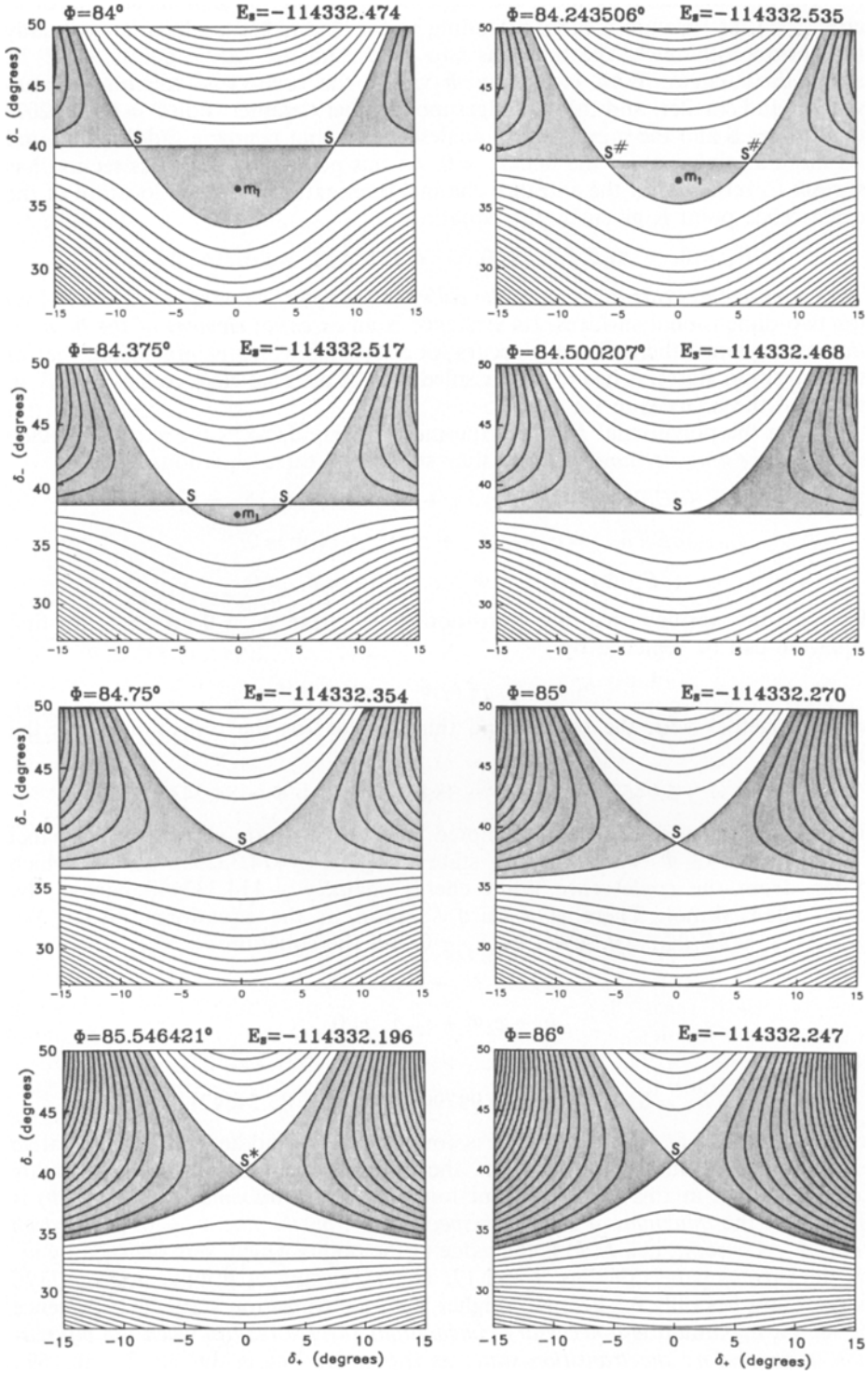
Φ=84° E_s=−114332.474
Φ=84.243506° E_s=−114332.535
Φ=84.375° E_s=−114332.517
Φ=84.500207° E_s=−114332.468
Φ=84.75° E_s=−114332.354
Φ=85° E_s=−114332.270
Φ=85.546421° E_s=−114332.196
Φ=86° E_s=−114332.247
δ_- (degrees)
δ_+ (degrees)
S
S#
S*
m_1

After the maximum the saddle S continues to decrease until Φ reaches 133°, as has been mentioned in the discussion of Figs. 13 and 14 in Sect. 4 and as it also seen from Fig. 16.

It is readily verified that the two transition states, the coalescence point and the maximum of $\tilde{E}(\Phi)$ would all coincide if the coefficients would "accidentally" satisfy the determinant condition:

$$\begin{vmatrix} b_1 & b_2 & b_3 \\ c_{12} & c_2 & c_{23} \\ c_{13} & c_{23} & c_3 \end{vmatrix} = 0,$$

in which case we would have a *bifurcating transition state. This is close to being the case, since the three points lie, in fact, within* 0.34 *mhartree of each other. We have therefore a bifurcating transition region.* While the described surface topography conforms to the general rule [69] that a mathematically *exact* bifurcating transition state is very unlikely to occur, the deviation from this limiting case is sufficiently small that one has here a "*practical bifurcating transition state*".

6.2. Stereospecificity

Because of the symmetry of the reaction surface with respect to the conrotatory variable δ_+ there clearly exists no preference for the valley m_3 or the valley m_4 in Fig. 10 (top), when the reaction path branches in the bifurcation region. Both stereoisomeric products will therefore occur with equal probability, i.e., the reaction would *not* be stereospecific if one could distinguish the four hydrogens. From this we predict that the ring opening of the appropriately deuterium-substituted cyclopropylidene will *not* be stereospecific, aside from the *dynamic* stereospecificity due to the different masses of H and D in the kinetic energy tensor. We expect, furthermore, that in substituted cyclopropylidenes, where stereospecificity has been observed experimentally, it is probably not caused by covalent electronic interactions.

7. Variation of relaxed internal coordinates

As mentioned earlier, the geometry optimizations for each (Φ, δ_1, δ_2) triple yields the other twelve internal coordinates as functions of Φ, δ_1, δ_2. An examination of these functional dependences exhibits details about the geometry changes of the molecule during the reaction. The continuity or possible discontinuity of these functions in the neighborhood of the reaction path indicates whether the choice of Φ, δ_1, δ_2 as principal reaction coordinates is reasonable.

Fig. 17. Contours of $E(\Phi, \delta_+, \delta_-)$ for eight values Φ = constant in the bifurcating transition region. The energy E_s of the contour passing through the saddle point(s) S is listed in millihartree at the *top right* of each panel. The contour value increment is 0.5 millihartree on all panels. *Shaded regions*: downhill from saddle points. The saddles S* on the panel for $\Phi = 84.243506°$ are the transition states of the reaction. The saddle S* on the panel for $\Phi = 85.546421°$ is the maximum of the minima obtained for $E(\Phi, \delta_+, \delta_-)$ when Φ = constant, $\delta_+ = 0$ (see text)

Accordingly, a series of additional energy calculations were performed for several panels Φ = constant, in the neighborhood of that point (δ_1^0, δ_2^0) at which the reaction path intersects those panels. Eight additional points were chosen as defined by the relations:

$$\{(\delta_1 + \delta_2)/2 - (\delta_1^0 + \delta_2^0)/2\} = 0°, +5°, -5°,$$
$$\{(\delta_1 - \delta_2)/2 - (\delta_1^0 + \delta_2^0)/2\} = 0°, +5°, -5°,$$

effectively surrounding the intersection point. We shall not list the complete data [68] of all these calculations, but merely depict the essential results graphically.

7.1. The four C–H bond distances

Their values remain at 1.089 ± 0.011 Å throughout all of these calculations. Moreover, they change even less within each Φ = constant panel. Thus, the issue of discontinuity does not arise at all.

7.2. The two C–C bond lengths

We are interested in the bonds C_0–C_1 and C_0–C_2. Figure 18 displays a plot of the values of these two nonbreaking C–C bond lengths. The "fluctuation bars" show the fluctuation of these values within each Φ panel. They do not change enough for any question of discontinuity to arise. The equality of the two C–C bond lengths up to the bifurcation point is of course a consequence of the C_s symmetry. For very large Φ values, it is a consequence of the similarity to allene.

7.3. The four C–C–H bond angles

Figure 19 displays a plot of the values of these angles along the reaction path. The two bond angles above the CCC plane (C_0–C_1–H_1 and C_0–C_2–H_2) are drawn in bold lines, while the two angles below the CCC plane (C_0–C_1–H_1, and

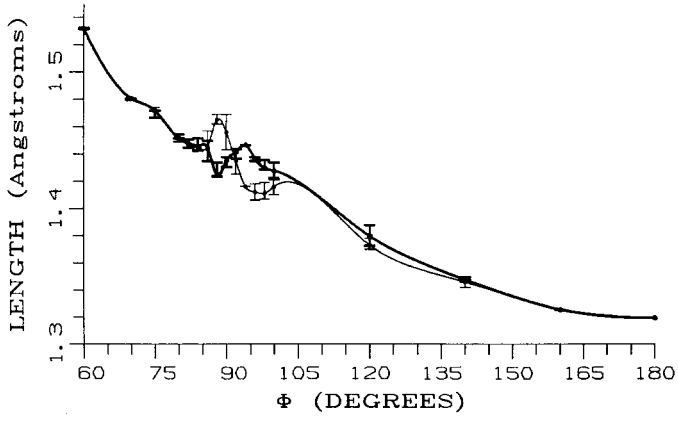

Fig. 18. Variation of bond distances C_0C_1 (*thick line*) and C_0C_2 (*thin line*) along reaction path

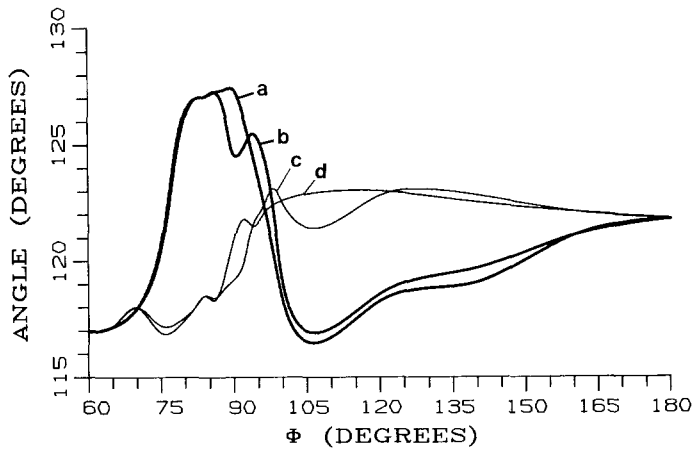

Fig. 19. Variation of CCH valence angles along reaction path **a** C_0–C_1–H_1; **b** C_0–C_2–H_2; **c** C_0–C_1–H_1; **d** C_0–C_2–H_2

C_0–C_2–$H_{2'}$) are drawn in thin lines. All deviations from smoothness occur near the transition region. No fluctuation bars are drawn, because the fluctuations of the values within a particular Φ panel are, in some cases, greater than the entire range shown in Fig. 19. These fluctuations can be seen from Fig. 20, which shows contours of the four bond angles as function of $\delta = (\delta_1 + \delta_2)/2$ and $\delta_- = (\delta_1 - \delta_2)/2$ for $\Phi = 60°$. This value of Φ = constant was chosen, because the fluctuations are by far the largest for this panel. There exist however no discontinuities. The overall changes are less than 10°. It is also interesting to note the symmetry of the changes, since the panels for the "top" bends are related to each other by a diagonal rotation around the $\delta_- = 0$ axis, while they are each related to the corresponding "bottom" bend by a rotation around the $\delta + \delta_- = 0$ axis.

7.4. The two C–C–H–H out-of-plane bends

Figure 21 depicts the changes in the values of the angles between each C–C bond and the corresponding CH_2 plane along the reaction path, as functions of Φ. In accordance with the C_s symmetry, the angles are seen to start out at exactly opposite values, and then change by equal and opposite amounts during the disrotatory C_s-preserving phase of the reaction until they both become equal to 0° near the transition region. From then on, they change in the same direction, although not always by the same amount. After the molecule has reached the slopes of the free synchronized CH_2 plane rotation valleys, the two bends become again approximately equal and remain so until the end of the reaction. The "fluctuation bars" indicate again the fluctuations of the angle values within each Φ panel. Some of these are fairly large. We therefore plot again values of the bends as functions of δ and δ_-. Contour plots for some Φ panels are shown in Fig. 22. They are selected from those showing the largest change. It is apparent that no discontinuities are present.

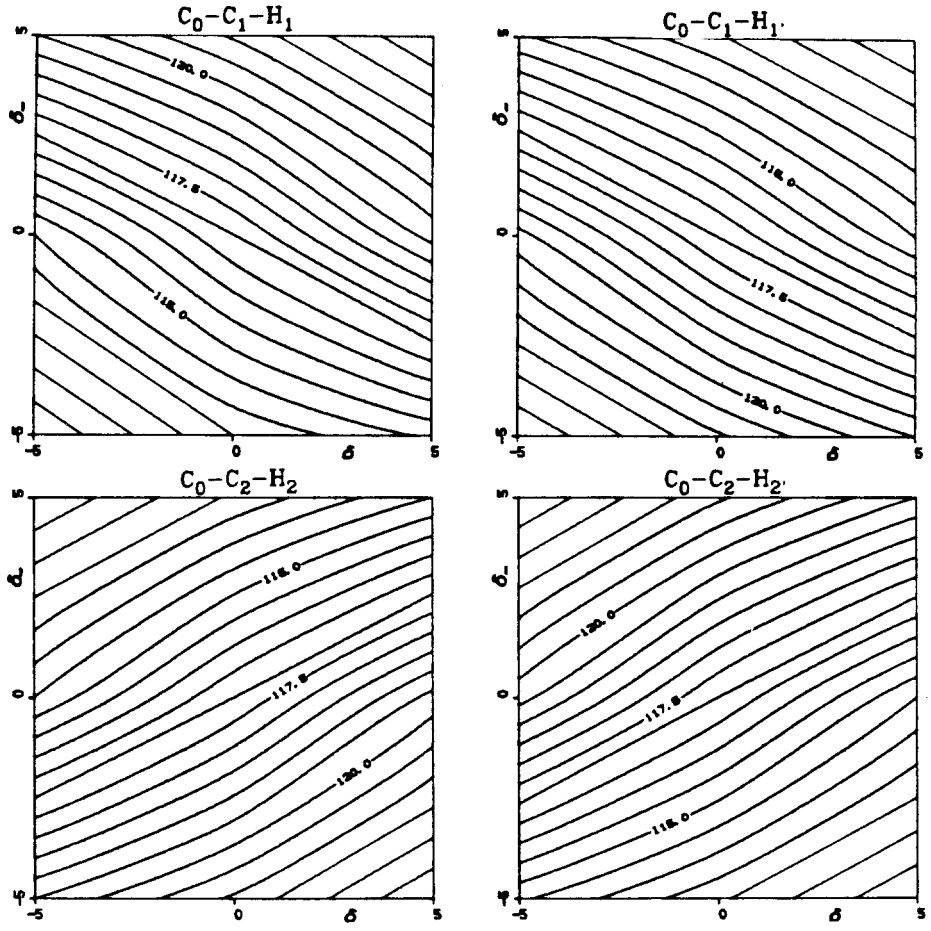

Fig. 20. Variation of CCH valence angles for $\Phi = 60°$ as function of δ_+ and δ_-. Contour value increments: 0.5°

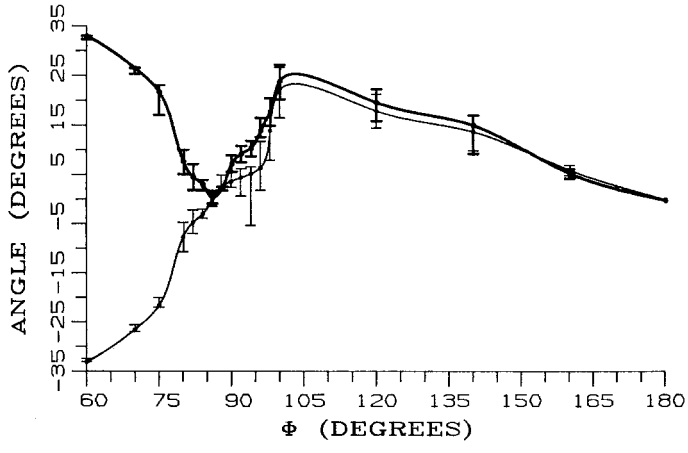

Fig. 21. Variation of C–CH_2 out-of-plane bending angles along reaction path. *Thick line*: C_0–C_1–H_1–H_1; *thin line*: C_0–C_2–H_2–H_2

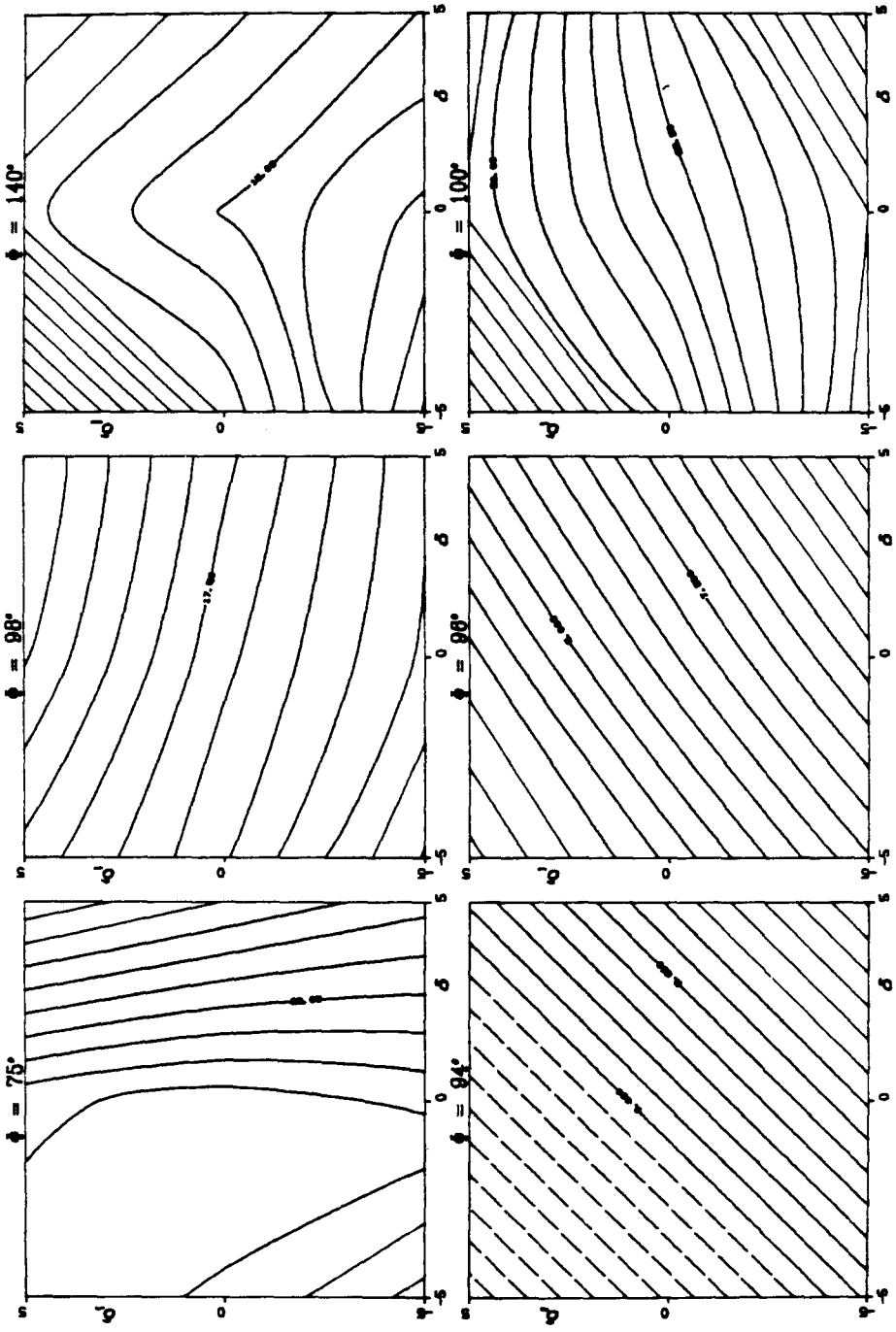

Fig. 22. Variation of C–CH_2 out-of-plane bending angles for values of Φ. Contour value increments: 0.5°

Figures 18–22 show that none of the twelve secondary internal coordinates exhibits abrupt changes along the presumed reaction path. It can therefore be concluded that the chosen variables (Φ, δ_1, δ_2) provide reasonable reaction space coordinates.

8. Conclusion

The potential energy surface governing the ring opening of cyclopropylidene has been globally mapped as a function of the ring-opening angle Φ and two angles δ_1, δ_2 describing the rotations of the two CH_2 groups. The latter were taken to be the dihedral angles between the CH_2 planes and the C_3 plane. For each (Φ, δ_1, δ_2) set, the remaining twelve internal coordinates were relaxed by energy minimization.

The reactant, singlet cyclopropylidene, was found to be stable for $\Phi \approx 60°$ with the two CH_2 groups standing perpendicular to the C_3 plane. Along the ring-opening reaction path, the CH_2 groups initially incline toward each other in a C_s-preserving, disrotatory manner as Φ increases. Shortly before Φ reaches 80°, with the CH_2 groups being inclined about 35° with respect to their original positions, a conrotatory component admixes as Φ opens further and C_s symmetry is lost. The conrotatory component can be clockwise or counterclockwise and the reaction channel bifurcates correspondingly. The two exit channels are each other's mirror images (assuming the hydrogens are distinguished by numbering) and lead to stereoisomeric products. No inherent preference exists for the two branches. On each branch, a transition state occurs very shortly after the bifurcation. The region encompassing the two transition states and the bifurcation can be considered as a "bifurcating transition region". The described progression of molecular geometries is illustrated in Fig. 23.

For ring-opening angles from about 95° to 180°, the surface furthermore exhibits isoenergetic valleys along the lines $\delta_1 + \delta_2 = \pm 90°$ which imply synchronized free rotations of the two CH_2 groups in a cogwheel-type fashion. The molecule is therefore extremely floppy with respect to these internal rotations while moving downhill on the reaction paths from the transition states to the products.

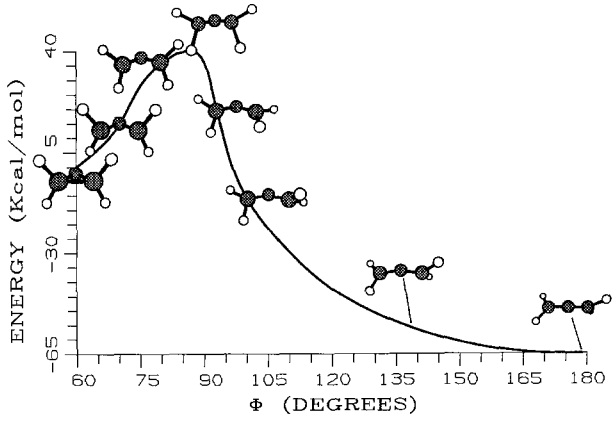

Fig. 23. Evolution of the molecular geometry along the reaction path from cyclopropylidene to allene

This description of the reaction will be refined in the third paper [73] by more accurate calculations of the key regions. They will provide a more detailed and somewhat modified picture of the bifurcating transition region. Also, the ring-opening barrier, shown in Fig. 23, will be lowered to less than 10 kcal/mol.

Acknowledgements. The authors wish to acknowledge that this investigation originated from Professor P.M. Warner pointing out to them the considerable interest which physical organic chemists have in understanding the reaction path of this ring opening.

References

1. Almenningen A, Bastiansen O, Traetteberg M (1959) Acta Chem Scand 13:1699
2. Angus RO Jr, Schmidt MW, Johnson RP (1985) J Am Chem Soc 107:532
3. Binkley JS, Pople JA, Hehre WJ (1980) J Am Chem Soc 102:939
4. Bodor N, Dewar MJS, Maksic ZB (1973) J Am Chem Soc 95:5245
5. Borden WT (1967) Tetrahedron Lett 5:447 and a widely quoted private communication
6. Carsky P, Urban M (1980) In: Berthier G, Dewar MJS, Fischer H, Fukui K, Hartmann H, Jaffe HH, Jortner J, Kutzelnigg W, Ruedenberg K, Scrocco E, Zeil W (eds) *Ab initio* calculations, methods and applications in chemistry. Springer, Berlin Heidelberg New York
7. Chapman OL (1974) Pure Appl Chem 40:511
8. Cheung LM, Sundberg KR, Ruedenberg K (1979) Int J Quantum Chem 16:1103
9. Dillon PW, Underwood GR (1977) J Am Chem Soc 99:2435
10. Dombek MG (1977) PhD Dissertation, Iowa State University and Ruedenberg K (1978) Proceedings of Workshop on Post-Hartree–Fock Methods, National Resource for Computation in Chemistry, Lawrence Berkeley Laboratory, University of California
11. Dupuis M, King HF (1978) J Chem Phys 68:3998
12. Dupuis M, Spangler D, Wendoloski JJ (1980) Nat Resour Comput Chem Software Cat. 1, Prog. No. QG01 (GAMESS)
13. Dykstra CE (1977) J Am Chem Soc 99:2060
14. Dykstra CE, Schaefer HF III (1980) In: Patai S (ed) The chemistry of ketenes, allenes and related compounds. Wiley, Interscience, New York, p 1 and references therein
15. Edmiston C, Ruedenberg K (1963) Rev Mod Phys 35:457
16. Elbert ST, Cheung LM, Ruedenberg K (1980) Nat Resour Comput Chem Software Cat 1, Prog. No. QM01 (ALIS)
17. Elbert ST, Ruedenberg K (to be published)
18. Feller DF (1979) PhD Dissertation, Iowa State University
19. Feller DF, Schmidt MW, Ruedenberg K (1982) J Am Chem Soc 104:960
20. Fukui K (1981) Int J Quantum Chem 515:633–42
21. Hariharan PC, Pople JA (1973) Theor Chim Acta 28:213
22. Hegelund F, Duncan JL, McKean DC (1977) J Mol Spectrosc 65:366
23. Hehre WJ, Ditchfield R, Pople JA (1972) J Chem Phys 56:2257
24. Hehre WJ, Ditchfield R, Stewart RF, Pople JA (1970) J Chem Phys 52:2769
25. Hehre WJ, Stewart RF, Pople JA (1968) Symp Faraday Soc 2:15
26. Hehre WJ, Stewart RF, Pople JA (1969) J Chem Phys 51:2657
27. Herzberg G (1966) Electronic spectra of polyatomic molecules. Van Nostrand Reinhold, New York
28. Honjou N, Pacansky J, Yoshimine M (1984) J Am Chem Soc 106:5361
29. Honjou N, Pacansky J, Yoshimine M (1985) *Ab initio* studies of the C_3H surface: I. SCF and CI study of structures and stabilities of isomers. J Am Chem Soc :
30. Ishida K, Morokuma K, Komornicki A (1977) J Chem Phys 66:2153–6
31. Johnson RP, private communication
32. Johnson RP, Schmidt MW (1981) J Am Chem Soc 103:3244
33. Jones WM, Krause DL (1971) J Am Chem Soc 93:551
34. Jones WM, Walbrick JM (1969) J Org Chem 34:2217

34. Jones WM, Walbrick JM (1969) J Org Chem 34:2217
35. Jones WM, Wilson JW Jr (1965) Tetrahedron Lett 21:1587
36. Jones WM, Wilson JW Jr, Tutwiler FB (1963) J Am Chem Soc 85:3309
37. Krogh-Jespersen K (1982) J Comp Chem 3:571
38. Lam B (1984) PhD Dissertation, Iowa State University
39. Lam B, Johnson RP (1983) J Am Chem Soc 105:7479
40. Lord RC, Venkatesvarlu P (1952) J Chem Phys 20:1237
41. Liu X, Ruedenberg K (to be published)
42. McIver JW Jr, Komornicki A (1971) Chem Phys Lett 10:303
43. McIver JW Jr, Komornicki A (1972) J Am Chem Soc 94:2625
44. Maki AG, Toth RA (1965) J Mol Spectrosc 17:136
45. Møller C, Plesset MS (1934) Phys Rev 46:618
46. Pasto DJ, Haley M, Chipman DM (1978) J Am Chem Cos 100:5272
47. Pople JA, Binkley JS, Seeger R (1976) Int J Quantum Chem Symp 10:1
48. Rauk A, Bouma WJ, Radom L (1985) J Am Chem Soc 107:3780
49. Roos BO (1980) Int J Quantum Chem 14:175
50. Roos BO, Taylor PR, Siegbahn PEM (1980) Chem Phys 48:157
51. Roth WR, Ruf F, Ford PW (1974) Chem Ber 107:48
52. Ruedenberg K (1971) Phys Rev Lett 27:1105
53. Ruedenberg K, Cheung LM, Elbert ST (1979) Int J Quantum Chem 16:1069
54. Ruedenberg K, Schmidt MW, Gilbert MM, Elbert ST (1982) Chem Phys 71:41 51 and 65
55. Ruedenberg K, Poshusta R (1972) Adv Quantum Chem 6:267
56. Ruedenberg K, Sundberg KR (1976) In: Calais JL, Goscinski O, Linderberg J, Ohrn Y (eds) Quantum Science. Plenum Press, New York, p 505; Ruedenberg K (1978) Proceedings of Workshop on Post-Hartree–Fock Methods, National Resource for Computations in Chemistry, Lawrence Berkeley Laboratory, University of California; Sundberg KR (1975) PhD Dissertation, Iowa State University
57. Runge W (1980) In: Patai S (ed) The chemistry of ketenes, allenes and related compounds. Wiley, Interscience, New York, p 45 and references therein
58. Salmon WI, Cheung LM, Ruedenberg K (1972) J Chem Phys 57:2776 and 2787
59. Schlegel HB (1982) J Comp Chem 3:214
60. Schmidt MW (1982) PhD Dissertation, Iowa State University
61. Schmidt MW, Gordon MS, Dupuis M (1985) J Am Chem Soc 107:2585–9
62. Seeger R, Krishnan R, Pople JA, Schleyer P von R (1977) J Am Chem Soc 99:7103
63. Siegbahn PEM, Almlof J, Heiberg A, Roos BO (1981) J Chem Phys 74:
64. Siegbahn PEM, Heiberg A, Roos BO, Levy B (1980) Physica Scripta 21:323
65. Staemmler V (1977) Theor Chim Acta 45:89
66. Stewart RJ (1970) J Chem Phys 52:431
67. Stierman TJ, Johnson RP (1985) J Am Chem Soc 107
68. Valtazanos P, Elbert ST, Ruedenberg K (1986) J Am Chem Soc 108:3147–3149
69. Valtazanos P, Ruedenberg K (1985) Theor Chim Acta 69:281–307
70. Valtazanos P, Ruedenberg K (1991) Theor Chim Acta 78:307 (Paper 4)
71. Walbrick JM, Wilson JW Jr, Jones WM (1968) J Am Chem Soc 90:2895
72. Wilson EB, Decius JC, Cross PC (1955) Molecular vibrations. McGraw-Hill, New York
73. Xantheas S, Ruedenberg K (1991) Theor Chim Acta 78:365 (Paper 3)
74. Xantheas S, Valtazanos P, Ruedenberg K (1991) Theor Chim Acta 78:327 (Paper 2)
75. Yaffe LG, Goddard WA (1976) Phys Rev A 13:1682